TITLE

Genetic insights into foveal morphology and its associations with pigmentation and age-related macular degeneration

AUTHOR LIST & AFFILIATIONS

David J. Green[1], David Romero-Bascones[2], Thomas H. Julian[1,3-5], Sofia Torchia[5], Heer N.V. Joisher[6-8], UK Biobank Eye and Vision Consortium, Unai Ayala[2], Maitane Barrenechea[2], Jay E. Self[9,10], Graeme C. Black[1,11], Tomas Fitzgerald[5], Ewan Birney[5], Constance L. Cepko[6-8], Joseph Carroll[12,13], Panagiotis I. Sergouniotis[1,3,5,11]

[1] Division of Evolution, Infection and Genomics, School of Biological Sciences, Faculty of Biology, Medicine and Health, University of Manchester, Manchester, UK.

[2] Biomedical Engineering Department, Faculty of Engineering (MU-ENG), Mondragon Unibertsitatea, Mondragón, Spain.

[3] Manchester Royal Eye Hospital, Manchester University NHS Foundation Trust, Manchester, UK.

[4] Christabel Pankhurst Institute, The University of Manchester, Manchester, UK

[5] European Molecular Biology Laboratory, European Bioinformatics Institute (EMBL-EBI), Wellcome Genome Campus, Cambridge, UK

[6] Department of Genetics, Blavatnik Institute, Boston, MA, USA

[7] Department of Ophthalmology, Harvard Medical School, Boston, MA, USA

[8] Howard Hughes Medical Institute, Chevy Chase, MD, USA

[9] Clinical and Experimental Sciences, Faculty of Medicine, University of Southampton, Southampton, UK

[10] Southampton Eye Unit, University Hospital Southampton NHS Foundation Trust, Southampton, UK

[11] Manchester Centre for Genomic Medicine, Saint Mary's Hospital, Manchester University NHS Foundation Trust, Manchester, UK

[12] Cell Biology, Neurobiology and Anatomy, Medical College of Wisconsin, Milwaukee, WI, USA

[13] Ophthalmology and Visual Sciences, Medical College of Wisconsin, Milwaukee, WI, USA

Correspondence to Panagiotis I. Sergouniotis (panagiotis.sergouniotis@manchester.ac.uk).

ABSTRACT

The fovea is the small depression at the neurosensory retina that underlies high-resolution central vision. It is vulnerable to disease and disruption of its architecture causes visual disability. Foveal morphology varies significantly across individuals. The molecular causes and functional consequences of this anatomical diversity are incompletely understood. Here, we extracted six foveal morphological parameters from Optical Coherence Tomography (OCT) images of 55,604 UK Biobank participants. We found notable variability in foveal morphology, and detected significant links with sex and genetic ancestry. Genome-wide association studies identified 197 lead loci across the six foveal morphological parameters, implicating genes involved in pigmentation (e.g., *TYR*, *TSPAN10, GPR143*) and patterning (e.g., *FGFR2*, *PTPRD, CYP1A1*). Heritability estimates ranged from 29-43%. Foveal pit volume was associated with future risk of age-related macular degeneration (HR>3.5, p=0.001), a finding supported by Mendelian randomization. These results establish foveal morphology as a highly-heritable trait with substantial influence over retinal disease risk.

INTRODUCTION

The fovea is a specialized structure at the center of the retina. It has a key role in high-acuity vision, supports most daily life activities, and enables tasks such as reading and face recognition.[1,2] The fovea is affected in a range of retinal disorders, including common adult-onset diseases such as age-related macular degeneration (AMD) (which is associated with loss of foveal cells) and pediatric conditions like albinism (which is characterized by foveal hypoplasia).[2]

The fovea has been the subject of study for more than a century. Despite this, there are significant gaps in our knowledge, partly because animal models that are routinely used in research (e.g. most murine and teleost models) lack this morphological specialization.[2] Recent advances in genomics, data science and *in vivo* imaging technologies have transformed our ability to study complex biological structures like the fovea.[3] Another major enabler has been the increasing availability of large-scale cohorts with a rich phenotypic scope. One example is the UK Biobank, a biomedical resource containing in-depth genetic and health information from >500,000 individuals.[4] Many UK Biobank participants underwent enhanced phenotyping including visual function assessment (>130,000 volunteers) and imaging of the central retina (>84,000 volunteers);[5] the latter was obtained using optical coherence tomography (OCT), a non-invasive imaging modality that rapidly generates cross-sectional retinal scans at micrometre-resolution.[6]

The most prominent morphological feature of the human fovea is the pit, corresponding to a central excavation of the inner retinal layers. Previous imaging studies have highlighted substantial morphological variability in respect to the depth, width and volume of the pit.[1,7–11] This anatomical diversity is thought to arise from variations in foveal development. Indeed, a blunted or absent foveal pit is often seen in individuals born prematurely.[12] Differences in foveal morphological parameters (hereafter, foveal traits) have also been reported between male and female and among individuals with different ancestral backgrounds.[7,13,14]

Previous studies have sought to investigate the genetic architecture of OCT-derived retinal traits, including central retinal thickness, and inner and outer retinal layer thickness.[15–20] However, to date, a comprehensive analysis of the genetic determinants of foveal morphology has not been undertaken. Here, we sought to address this knowledge gap and to explore the association between foveal traits and common retinal conditions (Fig.1).

RESULTS

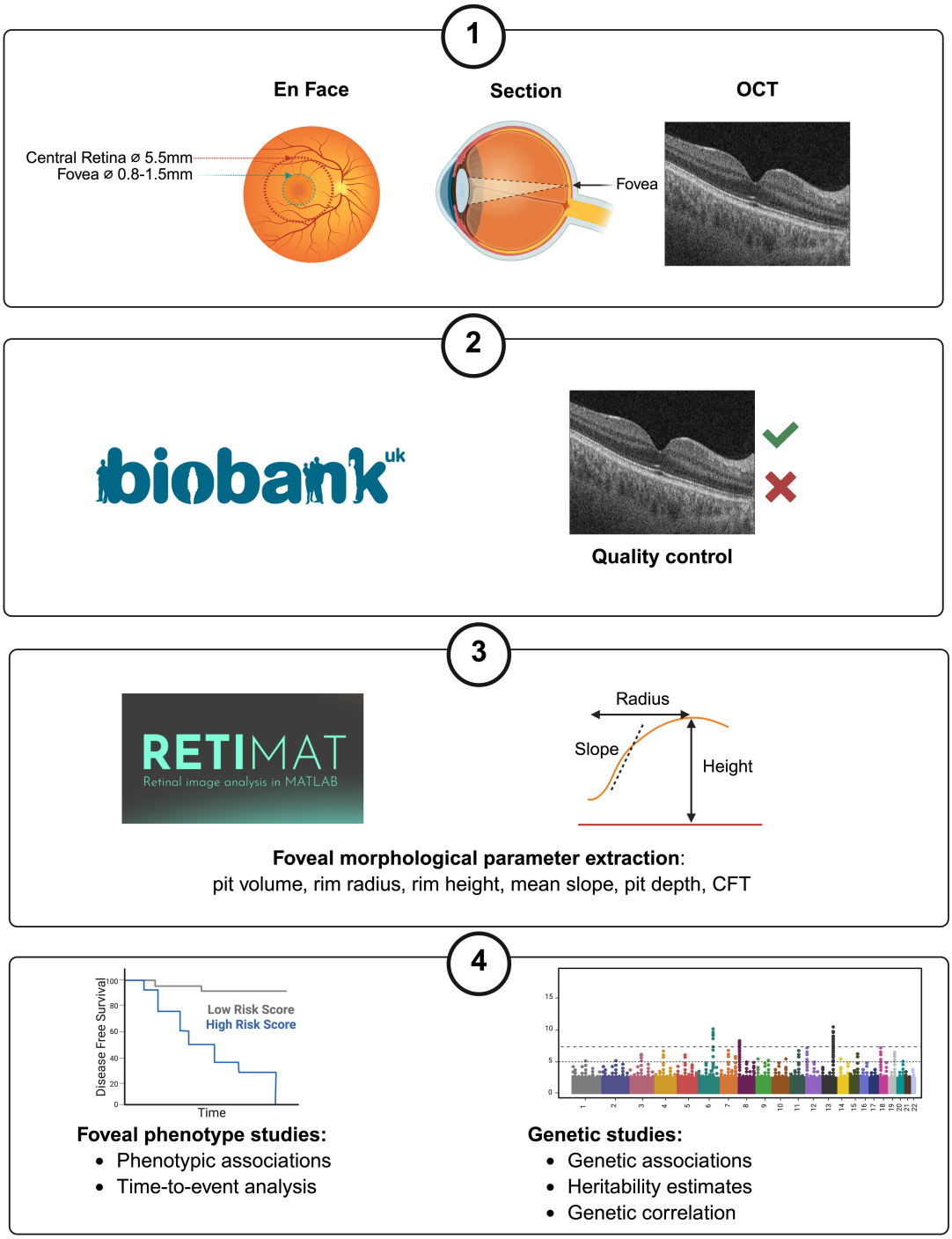

Fig.1. Outline of the study design. First, we used the RETIMAT tool to extract six key foveal traits from UK Biobank OCT scans (pit volume, rim radius, rim height, mean slope, pit depth and CFT). Subsequently, we performed phenotypic and genetic studies to gain insights into these foveal traits. Phenotypic analyses included the

investigation of the relationships between the studied foveal traits and age, spherical equivalent refractive error, sex, genetic ancestry, and visual acuity. Time-to-event analyses involved assessing the relationships between the six studied foveal traits and two major causes of visual impairment, age-related macular degeneration and glaucoma. Genetic investigations included common-variant genome-wide association studies (primary and replication), heritability estimation, and genetic correlation analyses.

OCT, optical coherence tomography; CFT, central foveal thickness.

112

113 **Phenotypic variability in foveal traits**

114 After applying standard OCT quality control filters,[20] we defined a subset of the
115 UK Biobank population with high-quality OCT scans. This cohort included 55,604
116 individuals and had similar sex and age profile to the overall UK Biobank
117 population.[15] Most study subjects were female (52%) and the mean age at OCT
118 imaging was 57.7 years (standard deviation: 8.1 years).
119
120 For each study subject, an OCT ‘volume scan’ (containing 128 cross-sectional
121 images) was available from the central retina of each eye. We used left eye
122 images as input to RETIMAT, an automated pipeline designed to extract foveal
123 traits from OCTs.[14] We focused on the following six parameters: foveal pit
124 volume, rim radius, rim height, mean slope, pit depth and central foveal thickness
125 (CFT) (Fig.1). The greatest fold range across UK Biobank participants was
126 observed for pit volume (15.1-fold), followed by pit depth (6.5-fold) and mean
127 slope (6.3-fold), indicating large differences between the most extreme
128 phenotypes in the population. In contrast, parameters such as rim height (1.4-
129 fold) and rim radius (2.1-fold) were more constrained (Fig.2).
130

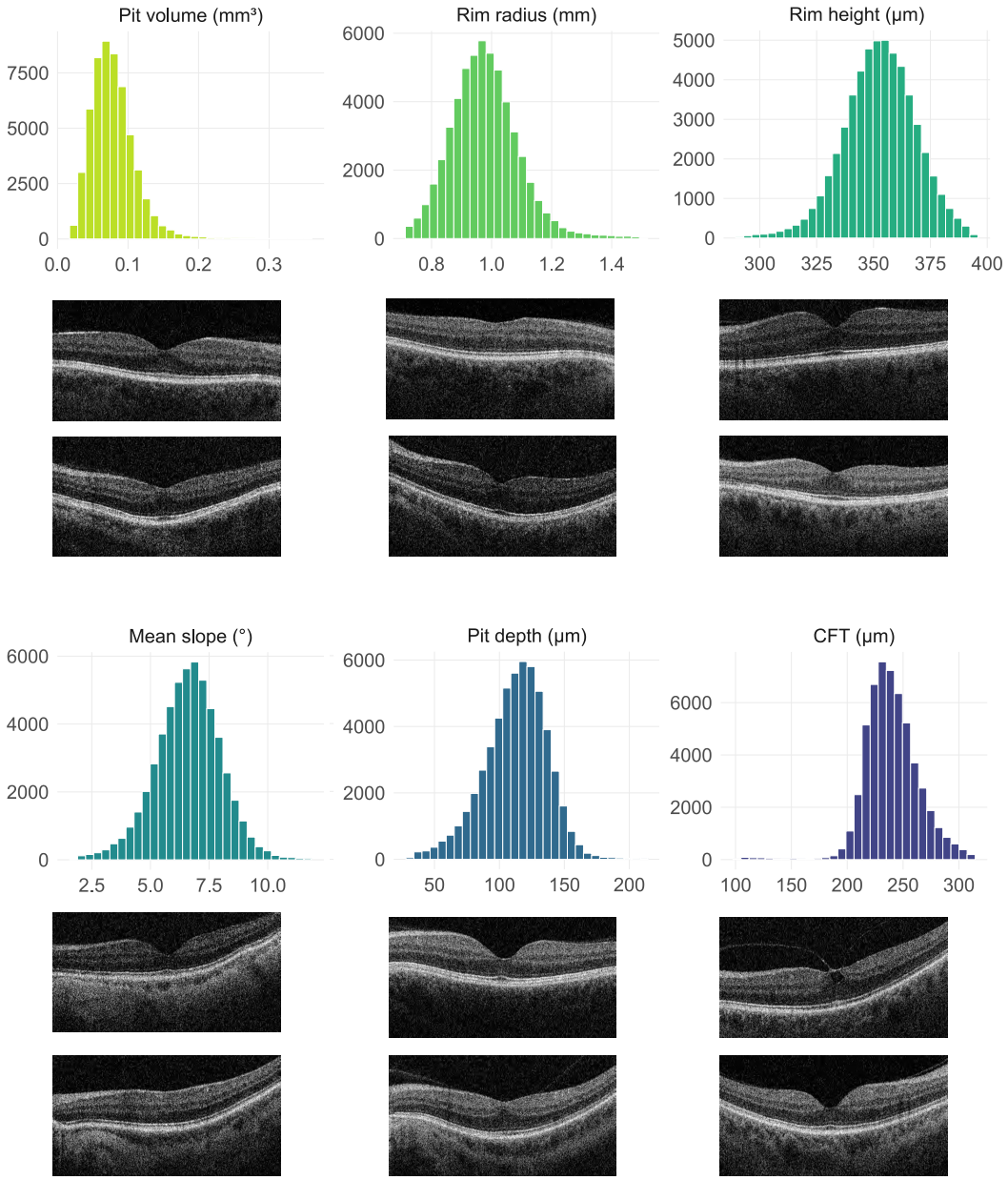

Fig.2. Histograms showing the distribution of six foveal traits in UK Biobank participants (after removal of 1% from the upper and lower tails of the data). Also shown are six examples of OCT scans from the extreme ends of each distribution. The following mean values were obtained: pit volume 0.080 mm^3 (range: 0.024–0.356 mm^3), rim radius 0.98 mm (range: 0.71–1.49), rim height 353 µm (range: 291–394 µm), mean slope 6.61° (range: 1.88–11.86°), pit depth 113 µm (range: 32–213 µm), central foveal thickness (CFT) 240 µm (range: 102–312 µm).

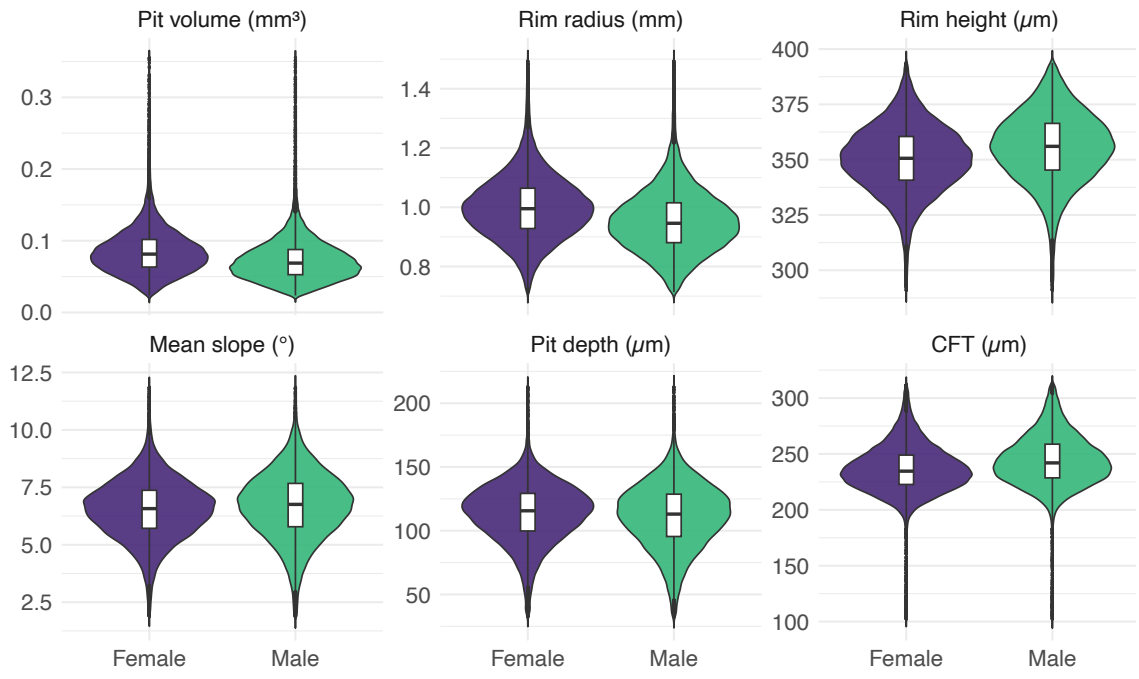

Fig.3. Violin plots showing the distribution of six foveal traits between male and female UK Biobank participants. Females tend to have larger pit volumes (0.085 mm^3 vs. 0.073 mm^3), deeper pits (114 µm vs. 111 µm) and slightly larger rim radii (1.00 vs. 0.954) than male. In contrast, male had higher central foveal thickness (CFT) (244 µm vs. 236 µm), steeper mean pit slopes (6.69° vs. 6.54°) and greater rim height (355 µm vs. 350 µm) than females. The Wilcoxon signed rank test was used to make comparisons and all p-values were found to be $< 2.3 \times 10^{-10}$. It is noted that the units for the foveal traits differ and, as such, the scales should not be directly compared. Further information, including numerical data, can be found in Supplementary Table S3.

First, we explored associations between the six studied foveal traits and age at image acquisition and found no notable correlations (Supplementary Table S1). We then examined associations between the same six foveal traits and spherical equivalent refractive error (a proxy for eye size) and found these to be variably correlated (Supplementary Table S2). Next, we inspected sex-related differences in foveal morphology, identifying statistically significant variation for all six studied traits. On average, females were found to have deeper, broader and larger foveal

pits than males (Fig.3; Supplementary Table S3). We also compared UK Biobank participants of different genetic ancestries, focusing primarily on individuals of European- and African-like ancestries (as these are the two largest groups in the dataset and the only two to contain >1,000 individuals; Fig.4; Supplementary Fig.S1; Supplementary Table S4). Again, we found statistically significant differences for all six studied foveal traits. On average, individuals of African-like genetic ancestries had deeper, broader and larger foveal pits that their European counterparts. These findings reinforce the role of sex and ancestry in shaping foveal morphology, and highlight the importance of including these parameters as covariates in subsequent genetic and phenotypic analyses of foveal traits.

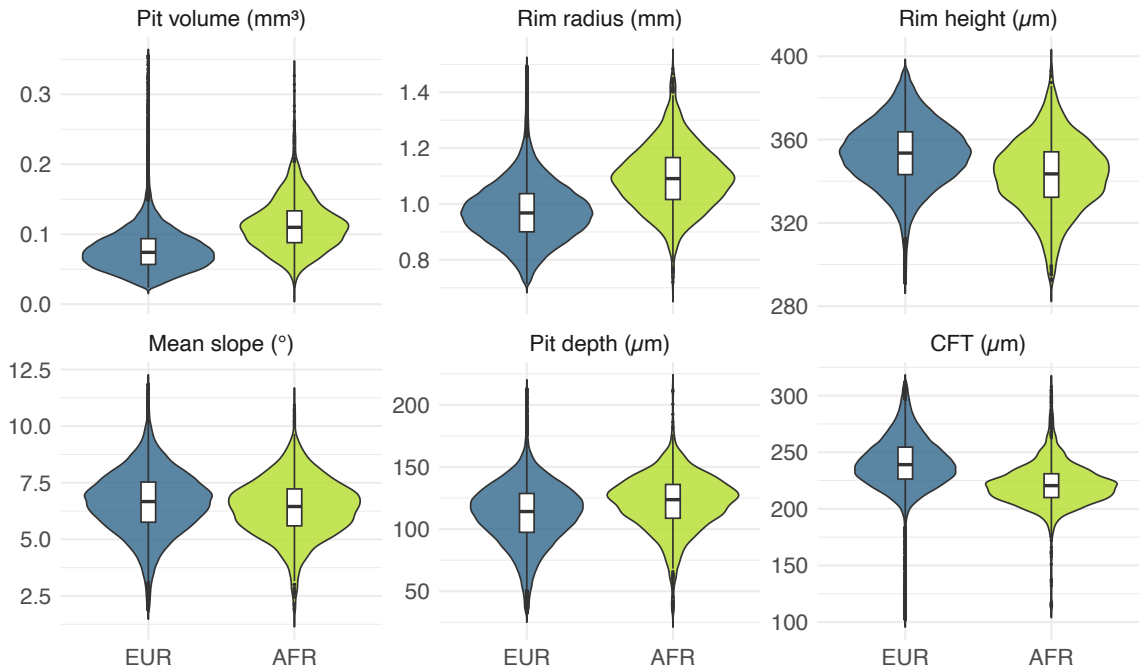

Fig.4. Violin plots showing the distributions of six foveal traits in individuals with European- and African-like genetic ancestries (EUR and AFR respectively). The AFR group had notably larger pit volumes (0.11 mm^3 vs. 0.08 mm^3), deeper foveal pits (121.37 µm vs. 112.19 µm) and greater rim radii (1.09 mm vs. 0.97 mm) than the EUR group. In contrast, the EUR group had higher central foveal thickness (240.65 µm vs 221.26 µm), steeper mean pit slope (6.62 ° vs. 6.41 °) and greater rim height (353.17 µm

vs. 342.80 μm) than the AFR group. The Wilcoxon signed rank test was used to make comparisons and all p-values were found to be $< 1 \times 10^{-10}$. It is noted that he units for the foveal traits differ and, as such, the scales should not be directly compared. Further information, including numerical data, can be found in Supplementary Table S4.

Aiming to gain insights into the factors underlying the detected differences between ancestral groups, we investigated the role of fundus (principally choroidal) pigmentation. To evaluate this, we used a fundus imaging-derived proxy of pigmentation, the 'Retinal Pigment Score' (RPS).[21] We then calculated the unique variance explained (adjusted R^2) values by RPS and ancestry across the six studied foveal traits, adjusting for age, sex and spherical equivalent refractive error. Overall, genetic ancestry explained a greater proportion of trait variance than fundus pigmentation for most traits, particularly pit volume and rim radius. It is noted that pigmentation explained negligible unique variance for rim radius, suggesting little independent contribution beyond genetic ancestry (Fig.5; Supplementary Table S5).

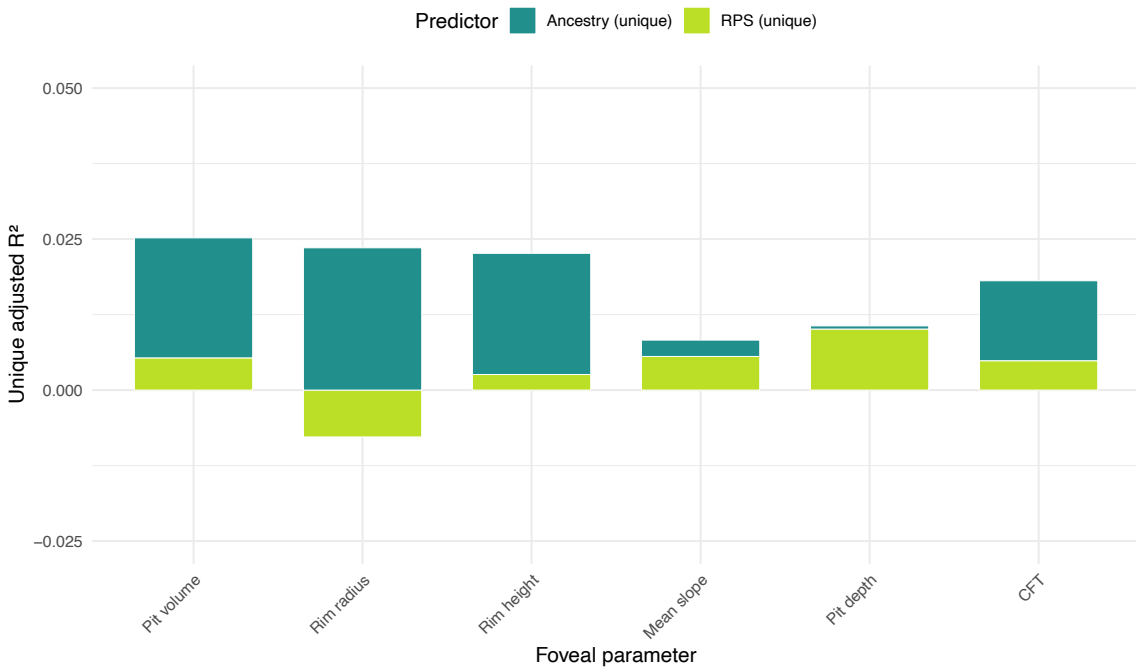

Fig.5. Unique contributions of fundus pigmentation and genetic ancestry to foveal morphology. Bar plots show the unique adjusted R^2 values for the six studied foveal traits, representing the proportion of variance explained by Retinal Pigment Score (RPS) and genetic ancestry, after adjusting for age, sex and spherical equivalent refractive error. Unique R^2 values were calculated from linear models by subtracting the R^2 of ancestry-only or RPS-only models from the combined model. Genetic ancestry accounted for a larger share of variance across most traits, particularly rim radius and pit volume (2.7% and 2.4% of variance, respectively). Pigmentation (RPS) explained modest additional variance, most notably for rim height and pit depth (0.9% and 0.6% of variance, respectively). For some traits, such as rim radius, the unique contribution of RPS was slightly negative, likely reflecting noise or model penalization rather than a true inverse effect. Further information, including numerical data, can be found in Supplementary Table S5.

To assess the extent to which foveal morphology predicts visual acuity, we performed linear regression with LogMAR vision as the outcome, and age, sex, spherical equivalent refractive error, and genetic ancestry as covariates. Several traits were significantly associated with acuity, but all effect sizes were small (R^2 < 1.3%). Mean slope was the strongest predictor, with steeper pits linked to

169 better vision. In contrast, greater pit volume was associated with worse acuity,
170 and central foveal thickness showed no effect (p = 0.30) (Supplementary Fig.S2).
171

172 **Association between foveal traits and risk of retinal disease**

173 To investigate whether foveal morphology constitutes a risk factor for future
174 retinal conditions, we performed Cox proportional hazards modeling using the six
175 studied foveal traits, along with time-to-event data for two leading causes of
176 visual impairment, AMD and glaucoma. We adjusted for age, sex, spherical
177 equivalent refractive error, and genetic ancestry in these analyses.
178
179 For AMD (n=1,345 cases), there was a notable association with larger pit volume
180 (hazard ratio 17.4; 95% confidence intervals [CI] 3.5-85.7) and wider rim radius
181 (hazard ratio 2.0; 95% CI 1.2-3.5). For glaucoma (n=1,166 cases), there were
182 statistically significant associations with mean slope, rim height and pit depth.
183 However, the corresponding hazard ratios indicated only small effect sizes
184 (ranging from 0.255 to 0.999) (Fig.6, Supplementary Table S6).

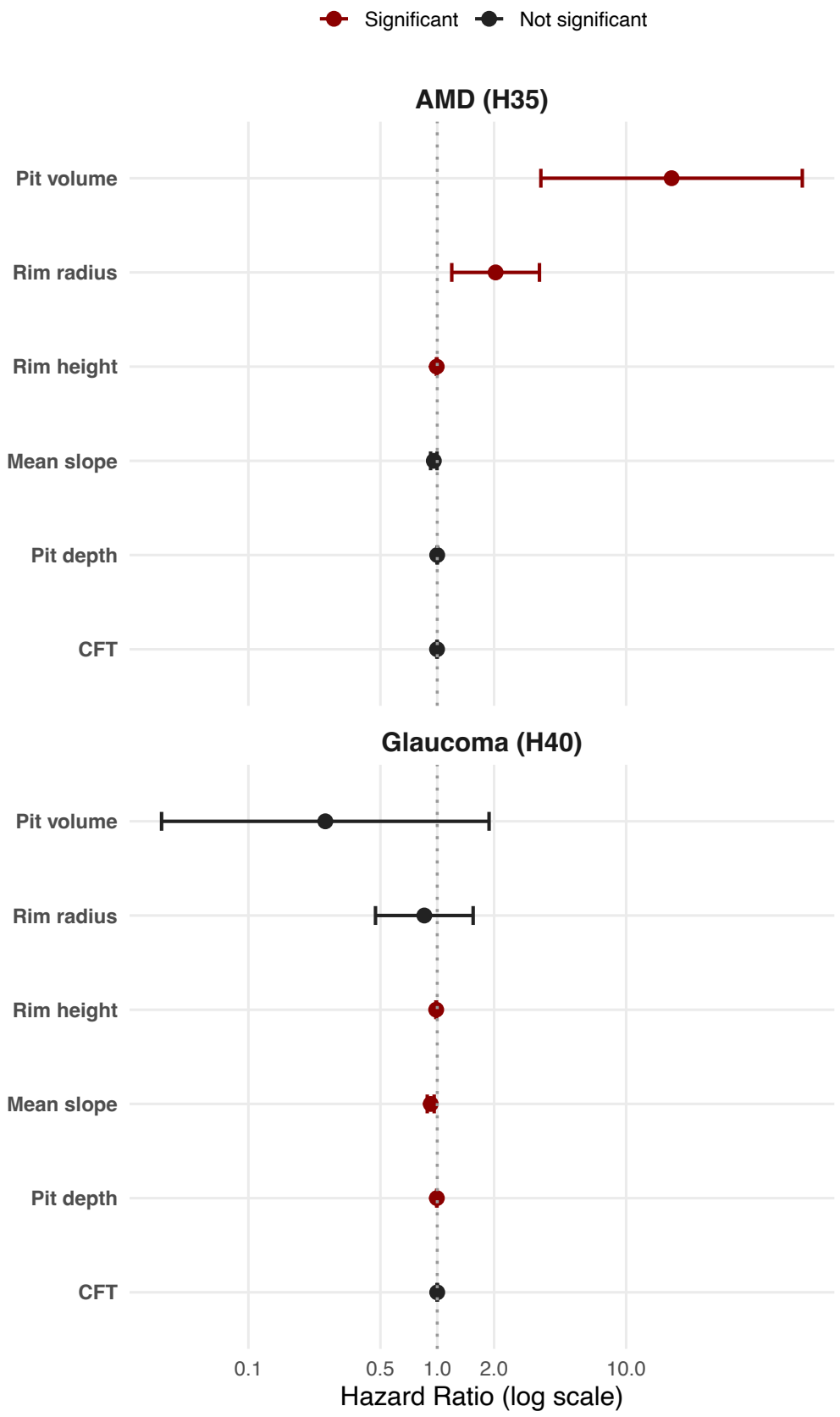
Significant
Not significant
AMD (H35)
Pit volume
Rim radius
Rim height
Mean slope
Pit depth
CFT
Glaucoma (H40)
Pit volume
Rim radius
Rim height
Mean slope
Pit depth
CFT
0.1
0.5
1.0
2.0
10.0
Hazard Ratio (log scale)

Fig.6. Cox regression analysis of associations between foveal traits and post-OCT-scan assigned codes for age-related macular degeneration (AMD) (H35) and glaucoma (H40). Statistically significant associations (after correcting for multiple comparisons using a 5% false-discovery rate [FDR] threshold) are highlighted with red. Further information, including numerical data, can be found in Supplementary Table S6.

Genetic associations of foveal traits

To investigate the genetic factors influencing the six studied foveal traits, we performed common-variant genome-wide association studies (GWAS) using REGENIE.[22] For these analyses, we defined a subset of the UK Biobank population that can be considered genetically well-mixed (*i.e.* includes participants that were assigned by genotype principal component analysis to a cluster with subjects of mostly European-like ancestries). After applying relevant imaging, genetic, and foveal trait quality controls, this cohort included 36,205 individuals; 29,710 of these were recruited between 2006 and 2010 (Instance 0, 'Initial assessment') and were used in the primary analysis while 6,495 were independently recruited between 2012 and 2013 (Instance 1, 'First repeat assessment visit') and were included in the replication study. The following covariates were incorporated into the models: age, sex, height, weight, spherical equivalent refractive error, and genetic principal components 1 to 20. We utilized a conventional threshold for multiple testing correction in GWAS studies, $p < 5 \times 10^{-8}$ ('genome-wide significance').

Genome-wide significant variants in the primary GWAS included: 5,933 for pit volume; 6,251 for rim radius; 7,694 for rim height; 4,117 for mean slope; 4,710

205 for pit depth; and 2,723 for CFT. Following analysis with GCTA-COJO
206 (conditional and joint multiple-variant analysis),[23] these merged into the following
207 lead loci: 64 for pit volume, 65 for rim radius, 45 for rim height, 29 for mean
208 slope, 40 for pit depth, and 28 for CFT (Fig.7, Supplementary Fig.S3-8;
209 Supplementary Dataset S1). We subsequently performed a replication GWAS
210 using UK Biobank subjects that were not included in the primary analysis,
211 establishing a high level of concordance between the primary and replication
212 studies with all traits having a correlation coefficient greater than 0.9
213 (Supplementary Fig.S9–14). Although the replication sample was considerably
214 smaller, several lead loci still reached genome-wide significance in both studies:
215 6 for pit volume, 4 for rim radius, 1 for rim height, 1 for mean slope, 2 for pit
216 depth, and 2 for CFT (Supplementary Dataset S1).
217
218 We identified a combination of trait-specific and shared loci influencing foveal
219 morphology. Many of these loci encompass variants previously linked to retinal
220 layer thickness parameters (including *TSPAN10* and *LINC00461*) while a subset
221 of them has been linked to monogenic disorders, most notably, albinism
222 (including *TYR*, *OCA2* and *GPR143*) (Table 1 and Supplementary Dataset S1).
223 Our primary analysis highlighted several loci that have not been previously
224 associated with retinal phenotypes, including *CYP1A1, PPP1R9A, KMT2A,*
225 *CASZ1* and *CCDC122*. We also identified variants in *FGFR2*, *PTPRD*, *SPRY2,*
226 *FLT1 and LATS1,* for which associations have only been detected for retinal
227 thickness measurements but not for foveal/macular traits.
228

MAGMA gene set enrichment analysis did not yield any statistically significant hits after correction for multiple testing.

It is noted that the genomic inflation factors (λGC) ranged from 1.12 to 1.17, with corresponding linkage disequilibrium (LD) score intercepts close to 1 (range: 1.005–1.027). These results suggest minimal confounding from population structure or cryptic relatedness. The attenuation ratios were uniformly low (all < 0.11), consistent with polygenic architecture and well-controlled inflation across all six studied traits (Supplementary Table S7).

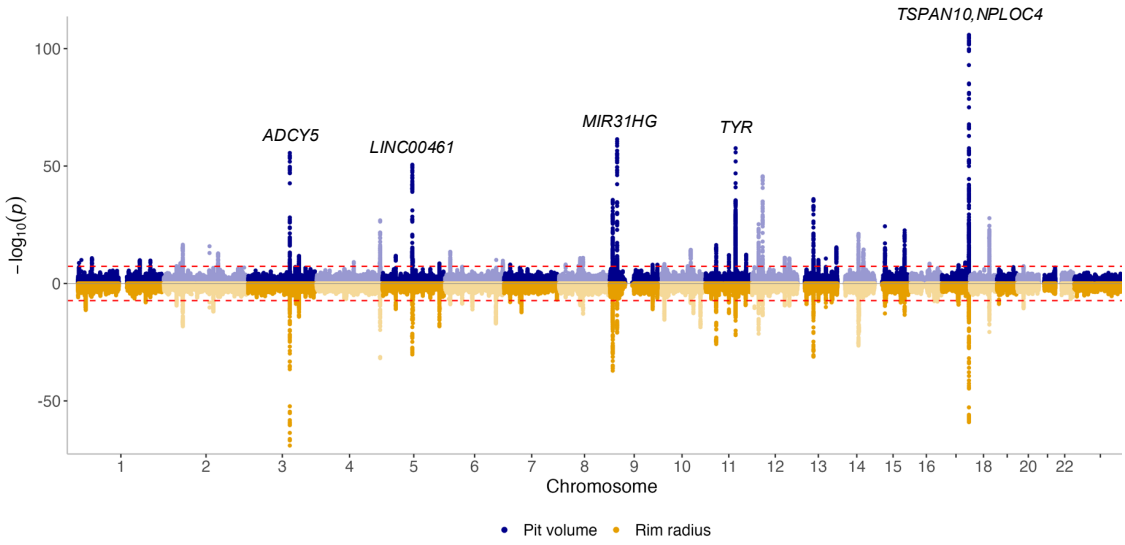

Fig.7. A Miami plot, illustrating the results of the primary genome-wide association study for foveal pit volume (top) and rim radius (bottom). The red line indicates the threshold for genome-wide significance, and 5 key loci exceeding this value have been annotated.

Heritability estimates for foveal traits

We used linkage disequilibrium (LD) score regression analysis[24] to obtain heritability estimates for the six studied foveal traits. We found moderate to high heritability, ranging from $h^2 = 0.29$ (standard error [SE] = 0.03) for CFT to $h^2 = 0.43$ (SE = 0.04) for pit volume. Rim height ($h^2 = 0.41$), rim radius ($h^2 = 0.39$), pit depth ($h^2 = 0.34$), and mean slope ($h^2 = 0.31$) were also significantly heritable (Supplementary Table S7).

Global genetic correlation between foveal traits

LD score regression was also used to assess the global genetic correlation between the studied traits. We found significant interdependence between many foveal traits. The strongest correlations (rg > 0.8) were observed between pit depth and mean slope (rg = 0.88) and between pit volume and rim radius (rg = 0.85), suggesting that these pairs reflect closely related biological processes. Moderate correlations (rg = 0.6-0.8) included pit depth and pit volume (rg = 0.76), mean slope and rim height (rg = 0.65), and pit depth and rim height (rg = 0.57), indicating shared underlying variation across several morphological aspects of the fovea.

In contrast, correlations between CFT and other parameters were more variable. We observed strong negative correlations between CFT and pit volume (rg = –0.79), pit depth (rg = –0.69), and rim radius (rg = –0.51), consistent with an

inverse relationship between retinal thickness and pronounced foveal pit excavation (Fig.8).

Correlations between foveal traits and fundus pigmentation (RPS) were generally weak (rg = -0.23 with pit depth, -0.22 with mean slope), with the strongest positive correlation seen with CFT (rg = 0.23) (Supplementary Table S8).

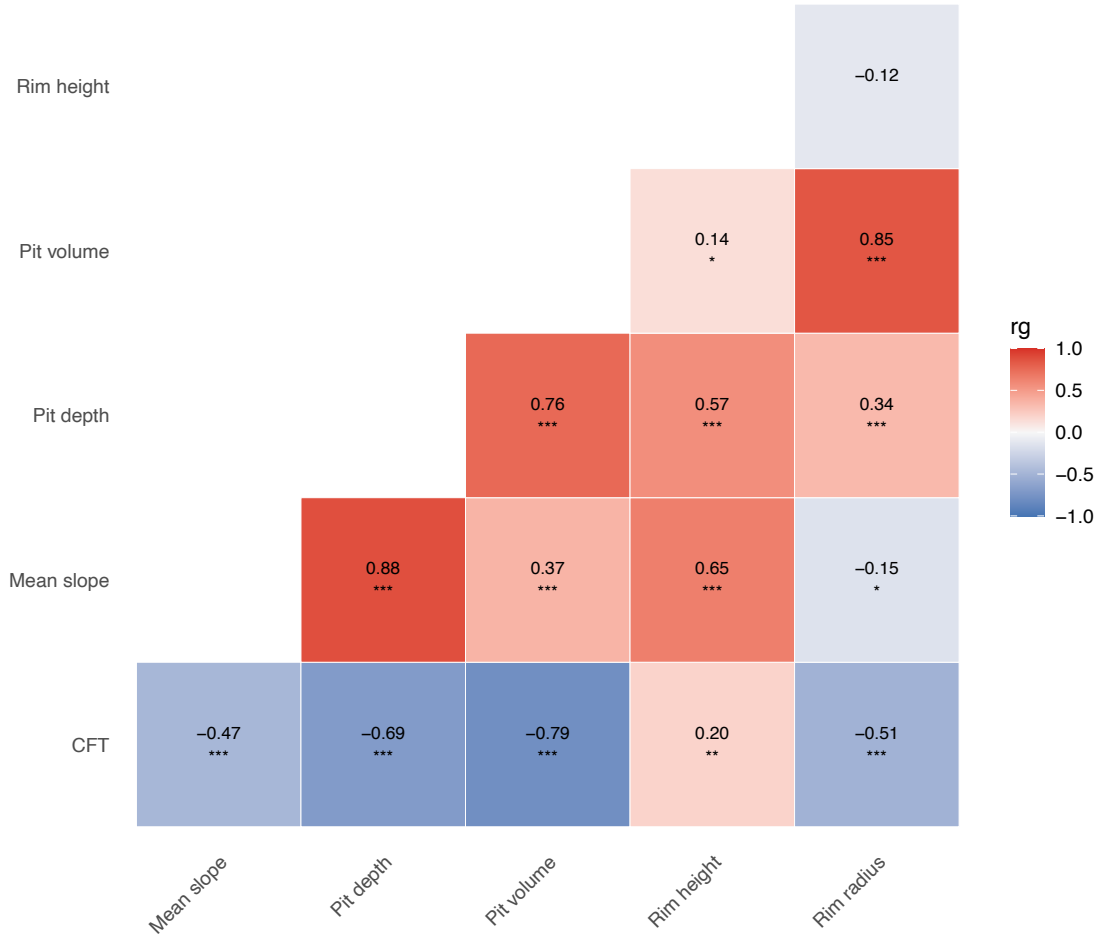

Fig.8. Genetic correlations between foveal traits. Asterisks indicate levels of statistical significance (* $p < 0.05$, ** $p < 0.01$, *** $p < 0.001$). Further information, including numerical data, can be found in Supplementary Table S8.

CFT, central foveal thickness.

Table 1. Summary of the 10 top-ranking loci associated with foveal traits**.**

Top-ranking common variant in locus	Chr: position (GRCh37)	Key gene(s)	Allele freq	Foveal trait with significant result (minimum p-value)	Selected previous associations in the GWAS Catalog; [Panelapp association(s)]
rs6420484	17:79612397	*TSPAN10 / NPLOC4 / PDE6G*	0.65	Pit depth (2.01×10^{-107}); Pit volume (7.41×10^{-105}); Rim radius (3.54×10^{-59}); Mean slope (3.16×10^{-55}); Rim height (4.88×10^{-48})	Retinal thickness measurements, refractive error, eye color, hair color
rs3138142	12:56115585	*RDH5 / CD63*	0.24	Rim height (1.98×10^{-77}); Pit depth (2.86×10^{-14}); Mean slope (6.21×10^{-13})	Retinal thickness measurements, refractive error, retinal vascular fractal density; [retinal dystrophy]
rs11708067	3:123065778	*ADCY5*	0.24	Rim radius (6.34×10^{-69}); Pit volume (7.95×10^{-56})	Retinal thickness measurements, height, birth weight, type 2 diabetes, glucose levels, HbA1c levels, cholesterol levels; [dyskinesia]
rs1042602	11:88911696	*TYR*	0.37	Pit depth (1.67×10^{-62}); Pit volume (8.26×10^{-58}); Rim radius (1.16×10^{-22}; Mean slope (3.48×10^{-39}); CFT (9.32×10^{-40});	Retinal thickness measurements, brain measurements, skin color, hair color; [albinism]
rs9298817	9:21576591	*MIR31HG*	0.66	Pit volume (1.43×10^{-61}); Rim radius (1.44×10^{-21}); Rim height (2.30×10^{-20})	Retinal thickness measurements, thyroid medication use
rs17421627	5:87847586	*LINC00461*	0.07	Pit volume (3.12×10^{-46}); CFT (1.34×10^{-35}); Rim radius (3.87×10^{-32}); Rim height (1.60×10^{-27})	Retinal thickness measurements, retinal vascular fractal density
rs11051145	12:31050201	*TSPAN11*	0.16	Pit volume (5.02×10^{-46}); CFT (5.22×10^{-34})	Retinal thickness measurements, optic disc size

rs7020703	9:8632149	*PTPRD*	0.22	Rim radius (1.25×10^{-37})	Retinal thickness measurements, bone mineral density, height, restless leg syndrome
rs67138036	4:187683202	*FAT1*	0.26	Rim radius (4.58×10^{-37})	Retinal thickness measurements; [microphthalmia/ coloboma, nephropathy]
rs1493523	15:44345614	*CCDC122*	0.68	Pit volume (1.86×10^{-36})	-

CFT, central foveal thickness

Mendelian randomization

We performed Mendelian randomization (MR) analysis on the two foveal traits that we found to be associated with significantly increased risk of AMD and glaucoma. This analysis revealed causal relationships between foveal morphology and retinal disease risk. There was evidence of causal association between increased pit volume and AMD (OR = 1.12, 95% CI: 1.04–1.21, inverse variance weighted [IVW] p = 0.004). This was robust to a leave-one-out test using the IVW method. In contrast, rim radius showed no evidence of a causal effect on AMD or glaucoma (p > 0.2 across all methods). Pit volume was also nominally associated with decreased risk of glaucoma (IVW p = 0.02; OR = 0.94, 95% CI: 0.89–0.99). This result remained significant in the MR Egger (p=0.02) and weighted mode (p=0.03) but did not quite exceed significance in the weighted median (p=0.056) nor persist throughout leave-one-out testing using the IVW method (Supplementary Table S9). Reverse Mendelian randomization analyses yielded no evidence of AMD or glaucoma influencing foveal morphology. Overall, the findings provide evidence that pit morphology causally influences the risk of AMD and primary open-angle glaucoma, but these results should be interpreted in the context of their reliance on several key assumptions of Mendelian randomization being met (see Methods for further details on this).

DISCUSSION

In the present study, we performed large-scale phenotypic and genetic analyses to better understand the variability and determinants of foveal morphology. By leveraging retinal imaging data from UK Biobank participants and a comprehensive foveal trait calculation tool (RETIMAT), we were able to detect differences in foveal morphology influenced by sex, genetic ancestry, and genetic factors. We also found a notable association between foveal pit volume and AMD.

We first analyzed how foveal architecture varies at the population level. As the number of subjects in this study is an order of magnitude greater than in most prior reports, we were able to identify previously unrecognized variability in foveal pit morphology (e.g. 15-fold for pit volume). Sex and ancestry were found to significantly influence foveal morphology, an observation that is in keeping with the findings of previous smaller-scale studies.[7,9,13,14] In line with previous research, males exhibited greater rim height, shorter rim radii, and a steeper mean slope.[14] Similarly, we found that individuals with African ancestries had wider, deeper, and more voluminous foveal pits than their European counterparts, in line with findings by Zouache *et al.*[7] The smaller East- and South-Asian ancestral groups fell between these two, consistent with the limited normative datasets available for Asian populations.[25,26] It is highlighted that, in contrast to most previous studies, we used genetic ancestry, a metric that is more accurate and objective than ethnicity or self-reported ancestry.[27] We also performed additional analyses to gain insights into the extent to which the

observed difference between continental groups is driven by pigmentation. Our observations suggest that genetic ancestry tends to be an independent contributor irrespective of fundus pigmentation, especially for foveal pit volume and rim radius.

We found that a larger pit volume is a key risk factor for AMD, and that there is a 33% increase in risk per 0.1 mm^3 increase in pit volume. This observation was supported by two orthogonal approaches, Cox regression analysis and Mendelian randomization. The results of the latter substantially reduce the risk that the observed association is due to reverse causation or confounding, and support the assertion that pit volume is a risk factor for AMD rather than a correlate. While the hazard ratio was 17.4 (95% CI 3.5-85.7), the corresponding odds ratio (OR) was 26.1 (95% CI 6.1-112.0, $p = 1.1 \times 10^{-5}$) (Fig.6, Supplementary Tables S6 and S10). It is noted that several environmental and genetic risk factors have been previously associated with AMD, including: age (OR 1.1), gender (OR 1.6), smoking (OR 1.9)[28], *CFH* gene variants (e.g. homozygosity for rs1061170 corresponds to OR of 4.7)[29], *ARMS2* locus variants (e.g. homozygosity for rs10490924 corresponds to OR of 8.6)[30] and family history (OR 10.8).[31] Although AMD selectively affects the foveal/macular region, to date, anatomical risk factors have been understudied[9] and, to our knowledge, this is the first time that specific foveal morphological parameters are found to set the stage for susceptibility to AMD. It can be speculated that the link between a larger pit and AMD risk is driven by differences in the distribution of macular xanthophyll pigments and/or by alterations in photoreceptor cell densities in the

vulnerable parafoveal area of low rod-to-cone ratio.[32] Future advanced ophthalmic imaging and mathematical modelling studies will provide further insights into how foveal anatomy predisposes to this leading cause of visual impairment.

Following phenotypic analyses, including of foveal traits that have received little attention so far (such as foveal volume and radius), we performed genetic association studies. We found that the observed morphological diversity has a strong genetic underpinning, with a high level of heritability across most traits (Supplementary Table 7). Pigmentation-related genes such as *TYR* and *TSPAN10* surfaced across multiple foveal traits, underscoring the role of melanin synthesis in the shared developmental pathways that shape foveal morphology (Table 1). This is in keeping with previous observations in albinism[33,34] and in a smaller cohort where a link between the common functional *TYR:*c.1205G>A (p.Arg402Gln) [rs1126809] variant and decreased rim radius was reported.[35]

While many of the lead loci detected here have previously been linked to retinal traits, at least 124 of them have no such prior associations (Supplementary Dataset S1). Two examples are *CYP1A1* and *PPP1R9A. CYP1A1* (lead marker: rs200391170; association with mean slope; $p = 2.2 \times 10^{-21}$) encodes a major cytochrome P450 enzyme and is involved in the metabolism of both endogenous substances and environmental chemicals. It has been implicated in the conversion of all-trans retinol to all-trans retinoic acid in human fetal tissues.[36] Notably, retinoic acid gradients are essential for dorsoventral patterning, and retinoic acid signaling has been directly linked to the positioning of the fovea-like

area in the chick retina.[37,38] Another gene that has not been previously linked to retinal phenotypes is *PPP1R9A* (lead marker: rs9649194; association with pit depth and mean slope; minimum $p = 6.5 \times 10^{-14}$). This gene encodes a protein phosphatase that modulates actin cytoskeleton organization,[39] and one possibility is that it plays a role in the formation of the foveal pit (rather than the patterning/positioning of this high-acuity structure to the correct retinal region, a process that occurs earlier in development).

A subset of the detected lead loci (n=36) has been previously linked to retinal thickness measurements (either clinically-used[15–17] or deep learning based[5,19,40]) but not with foveal/macular traits (Supplementary Dataset S1). These novel associations that we report here enhance the interpretability of the signals and allow more robust links to be drawn with central retinal development/patterning. Two notable examples are *FGFR2* and *PTPRD. FGFR2* (lead marker: rs146727842; association with mean slope; $p = 1.4 \times 10^{-20}$) encodes a receptor tyrosine kinase that is essential for embryonic development.[41] *FGFR2* has been shown to interact with *FGF8*, whose expression is required to pattern the chick fovea-like area.[37,38,42] *PTPRD* (lead marker: rs7020703; association with rim radius; $p = 1.3 \times 10^{-37}$) encodes a tyrosine phosphatase that regulates neural development by modulating receptor tyrosine kinase activity.[16,43] A related protein (cRPTPlambda) is found to be absent from the chick fovea-like area, and it can be speculated that *PTPRD* is involved in regulating FGF signaling early to set up the foveal region.[44]

This study has several limitations. First, obtaining accurate quantitative measurements of OCT-derived retinal features is inherently challenging. One issue is image scaling, as precise measurements require knowledge of the exact lateral scale of each scan. To address lateral magnification, we included spherical equivalent refractive error as a covariate in our analyses. While this method is less accurate than using ocular axial length[31,48], such measurements are not available in the UK Biobank dataset. It is noted though that our findings showed good agreement with those from smaller, more targeted studies.[47,49] This approach is also consistent with most previous genetic association studies involving retinal imaging-derived phenotypes.[15,16,18–20] Second, we relied on UK Biobank healthcare record data to identify cases of AMD and glaucoma. These records are known to be incomplete, and several alternative methods using retinal imaging data have been proposed.[50,51] Although these have shown positive diagnostic performance, they can overestimate prevalence,[51] and we opted to use a conventional approach focused on record-based diagnoses. Finally, while the UK Biobank was designed to be broadly representative of the ageing UK population, it is subject to selection biases. All reported associations should therefore be interpreted considering this limitation.[52,53]

In conclusion, we show that (i) foveal architecture is patterned by sex, genetic ancestry and genes related to pigmentation, and (ii) one aspect of that architecture, pit volume, appears to lie on the causal pathway to AMD. These findings position foveal pit metrics as potential biomarkers of macular

vulnerability and invite mechanistic work to dissect how developmental pathways intersect with ageing to drive retinal degeneration.

MATERIALS AND METHODS

Ethical approval

The UK Biobank has received approval from the UK National Information Governance Board for Health and Social Care and the National Health Service North West Centre for Research Ethics Committee (Ref: 11/NW/0382). This research was conducted using the UK Biobank Resource under projects 53144 and 49978. All investigations were conducted in accordance with the tenets of the Declaration of Helsinki.

UK Biobank: cohort characteristics and ophthalmic phenotyping

We used data from the UK Biobank, a resource containing genomic and health information from 502,355 individuals from across the United Kingdom, aged between 40 and 69 years at the time of recruitment.[3] Subsets of UK Biobank volunteers underwent enhanced phenotyping including visual acuity testing (>130,000 individuals), non-cycloplegic autorefraction (>125,000 individuals) and imaging of the central retina using color fundus photography and OCT (>84,000 individuals). Baseline ophthalmic assessment was conducted between 2009 and 2010 for most participants and between 2012 and 2013 for a smaller subset.[4]

Best-corrected visual acuity was assessed using a computer-displayed LogMAR chart (Precision Vision, LaSalle, IL, US) (UK Biobank data-fields: 5208 and 5201). Participants wore their habitual distance correction and were tested at 4 m; if unable to identify any letters, the chart was moved to 1 m. Starting from the top line, testing stopped once ≥2 letters on a line were misread.[4]

Non-cycloplegic autorefraction was carried out using a Tomey RC 5000 device (Tomey Corp., Nagoya, Japan). The spherical equivalent refractive error (spherical error + 0.5 ×

440 cylindrical error) was subsequently calculated for each participant (data-fields 5084-
441 5085; 5086-5087).[4]
442
443 Color fundus photographs and spectral-domain OCT images were acquired using the
444 Topcon 3D-OCT 1000 Mark II device (Topcon Corp., Tokyo, Japan), without
445 pharmacological dilation (data-fields 21015, 21016, 21011, 21013). OCTs were obtained
446 using a '3D macular volume' protocol (6 × 6 mm; 128 horizontal B-scans, each
447 comprising 512 A-scans arranged in a raster pattern).[5,40,54] The right eye was imaged
448 first. Our analysis focused on left eye images as we assumed that familiarity with the test
449 would have led to scans that, on average, had higher overall quality.[5,18]
450

451 **Fundus pigmentation quantification**

452 We used a recently described method[21] to evaluate fundus pigmentation in UK Biobank
453 participants. This involved calculating the Retinal Pigment Score (RPS), a continuous
454 quantitative metric that is thought to primarily reflect choroidal pigmentation.[55]
455
456 RPS was derived using the approach described by Rajesh *et al*. which entails selecting
457 fundus photographs of sufficient quality (*i.e.* those labeled as 'Good' by Automorph, an
458 established deep learning tool)[56] and processing them through the RPS pipeline to
459 quantify background pigmentation.[17]
460

461 **OCT quality control and foveal morphological parameter extraction**

462 OCT scans were filtered for overall quality in line with previous studies.[18,20] Briefly, we
463 discarded OCTs that (j) had a quality score below 40 and (ii) fell within the lowest 10%
464 of the inner limiting membrane (ILM) edge-strength indicator (a metric that captures the

465 sharpness and continuity of the ILM boundary and flags blinks, signal dropouts, and
466 major segmentation errors).[20]
467
468 OCT images meeting the above quality control criteria were processed using RETIMAT,
469 an open-source MATLAB toolbox for OCT image analysis. The processing pipeline
470 included the following steps:

471 • parsing Topcon (.fda) files to extract the ILM and Bruch's membrane (BM) surfaces
472 delineated by the device software;
473 • computing total retinal thickness maps;
474 • automatically aligning thickness maps to the foveal center;
475 • transforming raster thickness maps into a radial pattern; and
476 • computing morphometric values.

477
478 RETIMAT has been used successfully in previous studies and its fully automated
479 methods for fovea location and analysis have been independently assessed, making it
480 well-suited for high-throughput analysis.[14,57] We focused on six RETIMAT-derived foveal
481 traits: foveal pit volume, rim radius, rim height, mean slope, pit depth and central foveal
482 thickness (CFT) (Fig.1, Table 2).
483
484 Aiming to study the phenotypic variability of these parameters, we assembled a broad
485 'phenotypic analysis' cohort. This included UK Biobank participants whose OCT scans
486 passed the imaging quality control criteria for this study; whose RETIMAT-derived foveal
487 trait values did not fall in the 1% upper or lower extreme; and who were assigned to one
488 of the four main genetically-inferred ancestral groups (EUR, AFR, SEA, and SAS; see
489 'Genetic ancestry assignment' section below). Aiming to study the genetic architecture of
490 foveal traits, a second, more focused 'genetic analysis' cohort was defined. This was
491 limited to unrelated participants of European-like ancestries with OCT scans; no sex

492 chromosome aneuploidy; and not flagged as outliers for heterozygosity nor missingness.
493 Individuals with RETIMAT-derived foveal trait values exceeding 2.5 standard deviations
494 were also excluded (Supplementary Fig.S15); this cut-off was selected in accordance
495 with the approach used in previous genetic association studies of retinal thickness
496 measurements. [15,16,18–20] The final GWAS sample comprised 36,205 unrelated
497 individuals with European-like ancestries (29,710 primary plus 6,495 replication); the
498 broader phenotypic cohort totaled 55,604 individuals across ancestries.
499

Table 2. Definitions of the six RETIMAT-derived foveal traits analysed in this study

Foveal trait	Definition
Pit volume (mm^3)	Integrated volume between rim height and the full thickness profile
Rim radius (mm)	Radial distance from center to point of rim height
Rim height (µm)	Maximum thickness at the foveal rim
Mean slope (°)	Average inclination from center to rim
Pit depth (µm)	Rim height minus central foveal thickness
Central foveal thickness (µm)	Thickness at the foveal center

A pictorial representation of rim radius, rim height and mean slope can be found in Fig.1

500

501 **Genetic ancestry assignment**

502 To facilitate inter-ancestry analyses of foveal traits, we sought to characterize the
503 genetic ancestry of UK Biobank participants. A subset of 409,373 participants with
504 European-like ancestries is readily-available (data-field 22006) and we aimed to obtain
505 genetic ancestry estimates for the remaining 78,296 individuals. Using a previously-
506 described approach[58] we projected these UK Biobank participants onto reference
507 genetic data from the 1000 Genomes Project.[59] In brief, we used directly genotyped

single-nucleotide variants from the UK Biobank and genetic data from the 1000 Genomes Project (Phase 3, v5a.20130502). After matching variants between these two resources, we merged the two datasets using PLINK v2.0,[60] retaining 718,487 high-quality variants. We then performed linkage disequilibrium (LD) pruning and removed regions with long-range LD, resulting in 30,320 independent variants. Ancestry proportions were estimated using ADMIXTURE (v1.3.0),[61] with four reference groups from the 1000 Genomes Project dataset: GBR (European), YRI (African), ITU (South Asian), and CHS (East Asian). Only individuals with at least 80% ancestry probability assigned to one of these four groups were retained for further phenotypic analyses.

Statistical analyses of foveal phenotypes

The relationships between foveal traits, age of OCT image acquisition and spherical equivalent refractive error were studied using Spearman's correlation analyses. Further, comparisons were made between sex and genetic ancestry groups for each of the studied foveal traits using the Wilcoxon rank-sum test (when comparing two groups) and the Kruskal–Wallis test (when comparing more than two groups).

To quantify the contributions of fundus pigmentation (RPS) and genetic ancestry to variability in foveal morphology, we fitted linear regression models for each trait, as follows: The two predictors were analyzed together given their presumed biological relationship (as pigmentation traits vary by ancestry and may capture overlapping sources of variation).

Model 1: included RPS, spherical equivalent refractive error, and sex.

Model 2 included genetic ancestry (as a categorical variable), spherical equivalent refractive error, and sex.

Model 3: included both RPS and genetic ancestry terms, along with spherical equivalent refractive error and sex.

From each model, we extracted adjusted R^2 values to assess explained variance. Unique contributions of RPS and ancestry were derived by comparing the full model against models excluding one predictor set at a time.

Finally, the association between foveal morphology and visual acuity was studied using a linear regression approach with age, sex, spherical equivalent refractive error and genetic ancestry used as covariates.

Genome-wide association studies (GWAS)

We performed a common-variant GWAS using an additive linear model in REGENIE v3.1.1.[22] To meet the normality assumptions of GWAS, we applied rank-based inverse normal transformation to any foveal traits that deviated from a normal distribution. For this analysis, we focused only on individuals of European-like genetic ancestries (data-field 22006). We performed a primary and a replication GWAS. The focus of the former was on the 67,250 individuals that were imaged at the time of their baseline visit (Instance 0, 'Initial assessment visit (2006–2010)'). The focus of the replication study was on the 15,568 different participants that were imaged for the first time during their first repeat assessment (Instance 1, 'First repeat assessment visit (2012–2013)').

To process the imputed genotype data, we applied conventional quality control filters using PLINK2.[60] Variants were retained if they had: an imputation quality score above 0.8; a minor allele frequency (MAF) of 5% or more; and a minor allele count (MAC) of 20 or more. Variants with a Hardy-Weinberg equilibrium p-value below 1×10^{-15} were

excluded, along with those with missingness greater than 10%. Individuals with more than 10% missing genotypes were also excluded.[22]

The GWAS model was adjusted for age at recruitment (data-field 21022), sex (data-field 31), height (data-field 50), weight (data-field 21002), spherical equivalent refractive error (calculated from data-fields 5085 and 5086 and defined as spherical error + 0.5 × cylindrical error), and the first 20 genetic principal components (data-field 22009). Genome-wide statistical significance was set at $p < 5 \times 10^{-8}$.

To refine the obtained association signals, further analyses were performed using the GCTA-COJO tool (conditional and joint multiple-variant analysis).[23] Variants located on different chromosomes, or more than 10 Mb apart, were treated as unlinked. Lead genetic variants were then annotated using Ensembl,[62] Open Targets,[63] and GWAS Catalog[64] data (accessed on June 24, 2025). To accurately summarize the strongest signals, the LD metrics of the changes that were highlighted as lead variants by GCTA-COJO analysis and were within 1 Mb of one another were manually inspected using the LDlink tool.[65]

LD score regression: heritability estimation and global genetic correlation analysis

The global genetic correlations between the six studied foveal traits (pit volume, rim radius, rim height, mean slope, pit depth, and CFT) and RPS were calculated using LD score regression.[66] The GWAS summary statistics for RPS were obtained from a study by Julien *at al.*[55] The analysis adhered closely to the methodology described by Bulik-Sullivan *et al.*,[66] with genetic variants filtered according to the following criteria: inclusion in HapMap3; minor allele frequency > 0.01; imputation score > 0.9, exclusion of strand-

586 ambiguous variants; and removal of duplicated variants. LD scores were derived from
587 the European subset of the 1000 Genomes Project dataset.[59]
588
589 LD score regression was also used to calculate heritability, λ_G (genomic inflation factor),
590 intercept, and ratio (denoting the proportion of inflation resulting from confounding or
591 bias) for each of the six studied foveal traits.
592

593 **Cox regression analysis**

594 We performed Cox proportional hazards regression to investigate the association
595 between foveal traits and incident age-related macular degeneration (AMD) and
596 glaucoma. Participants with available OCT-derived foveal traits and outcome data were
597 included in the analysis (n = 55,604). Disease status was defined using hospital inpatient
598 ICD-10 diagnosis fields (data-field: 41202; ICD-10 H35 and H40). The date of baseline
599 imaging (Year of Scan, YOS) was extracted from UK Biobank data-field 21836 and used
600 to define time-zero for each participant.
601
602 Age at scan was computed from YOS and the month and year of birth for each
603 participant. We defined disease onset as the earliest recorded date for the relevant ICD-
604 10 code. Participants were censored at the last available follow-up date (May 31, 2022),
605 if their imaging date was missing, or if disease onset occurred before the scan.
606
607 Cox regression models were fitted using the 'lifelines' Python package,[67] with time-to-
608 event (in days) as the outcome, and foveal traits as the predictors. All models were
609 adjusted for age at image acquisition, sex, spherical equivalent refractive error, and
610 genetic ancestry. Ancestry was modelled using one-hot encoded genetic ancestry
611 categories with individuals of European-like ancestries as the reference group. Models

were fit for each trait–disease pair. Hazard ratios (HR), 95% confidence intervals, and p-values were extracted. The p-values were corrected for multiple testing using the Benjamini–Hochberg false discovery rate (FDR) method.

To enhance the interpretability of the detected associations, we performed logistic regression using a binary outcome defined as the presence or absence of disease onset after the scan date and before the censoring date (May 31, 2022). Individuals who had not developed the disease by the censoring date were treated as controls. Covariates included age at image acquisition, sex, spherical equivalent refractive error, and genetic ancestry (encoded as dummy variables). Analyses were run separately for each foveal trait. Logistic regression models were fitted using the 'statsmodels' Logit function in Python[68], and odds ratios (with 95% confidence intervals) and p-values were extracted.

Causal inference using two-sample Mendelian randomization

Causal associations between AMD, glaucoma and the six studied foveal traits were assessed using univariable two-sample Mendelian randomization (MR).[69,70] Population overlap biases univariable two-sample MR in the direction of causation. Accordingly, the populations contributing toward traits determined to be causal were inspected to ensure that there was no overlap. Genetic instruments were selected based on $p < 5 \times 10^{-8}$ in relation to each exposure trait. Where an exposure instrument was not present in the outcome dataset, we sought to identify a suitable proxy. Proxy variants were single-nucleotide variants that were in high LD with exposure-associated variants which were not present in the outcome dataset. Proxies were identified using the Ensembl server,[62] selecting variants with an LD R^2 value of 0.9 or above. Genetic variants were clumped using an LD R^2 value of 0.001 and a genetic distance cut-off of 10,000 Kb. This was achieved using the 1000 Genomes Project European superpopulation reference panel

638 and the TwoSampleMR PLINK clumping function.[59,60] The effects of instruments on
639 outcomes and exposures were harmonized to ensure that the β values (*i.e.* the
640 regression analysis estimates of effect size) were signed with respect to the same
641 alleles. For palindromic alleles (*i.e.* alleles that are the same on the forward as on the
642 reverse strand), those with minor allele frequency (MAF) > 0.42 were omitted from the
643 analysis to reduce the risk of errors due to strand issues. In addition to using a range of
644 Mendelian randomization methods and quality control measures (as detailed below), we
645 endeavored to remove pleiotropic instruments and outliers from the analysis. To achieve
646 this, instruments that were more statistically significant (in terms of p-value) for the
647 outcome than the exposure were removed. Radial Mendelian randomization,[71] an
648 approach that detects outlying instruments, was also used for outlier identification, and
649 outliers were subsequently removed.[71] The Cochran's Q test was performed for each
650 analysis. The MR Egger intercept[72] was used to detect horizontal pleiotropy. The I^2
651 statistic was calculated as a measure of heterogeneity between variant specific causal
652 estimates. An $I^2 < 0.9$ indicates that MR Egger is more likely to be biased towards the
653 null through violation of the “NO Measurement Error” (NOME) assumption. Our primary
654 analysis was a multiplicative random effects inverse variance weighted (IVW) test, which
655 is the most efficient analysis method with valid instrumental variables.[73] It is noted that
656 Mendelian randomization relies upon several assumptions holding true to provide an
657 accurate assessment of causation. The core assumptions are that (i) the instrumental
658 variables (single-nucleotide polymorphisms) utilized are associated with the exposure;
659 (ii) the instrumental variables are not associated with the outcome via a confounder; and
660 (iii) the instrumental variables do not impact the outcome other than through the
661 exposure being considered (*i.e.* no horizontal pleiotropy).[73] Robust analyses are those
662 which can provide valid causal inference under weaker assumptions than an IVW test,
663 and are important for a complete Mendelian randomization study. Robust tests included

the weighted median (robust to up to 50% of invalid instruments), weighted mode (robust to >50% of invalid instruments but assumes more variants estimate the true causal effect than estimate any other quantity), MR Egger (robust to pleiotropic effects of variants, provided the effects are independent of the variant-exposure associations) and a leave-one-out analysis using the MRE IVW method (to test for highly influential variants).[73] When appraising the results of a Mendelian randomization study, the confidence with which one can assert causality is influenced by both the strength of association in the primary analysis (IVW) and the range of robust tests in which the results are consistent. Where the IVW is significant but robust tests are not, this may be in keeping with causality, but under stricter assumptions of validity across the instrumental variables utilized (and therefore may warrant more cautious interpretation).

DATA AVAILABILITY

UK Biobank data are available under restricted access through a procedure described at http://www.ukbiobank.ac.uk/using-the-resource/. All other data supporting the findings of this study are available within the article (including its Supplementary Information files).

CODE AVAILABILITY

The scripts used to analyse the datasets included in this study are available at https://github.com/davidjohngreen/fovea and https://github.com/mu-biomed/retimat.

686 **REFERENCES**

687

688 1. Bringmann, A. *et al.* The primate fovea: Structure, function and
689 development. *Prog Retin Eye Res* **66**, 49–84 (2018).

690 2. Provis, J. M., Dubis, A. M., Maddess, T. & Carroll, J. Adaptation of the
691 central retina for high acuity vision: Cones, the fovea and the avascular
692 zone. *Prog Retin Eye Res* **35**, 63–81 (2013).

693 3. Meyer, H. V. *et al.* Genetic and functional insights into the fractal structure
694 of the heart. *Nature* **584**, 589–594 (2020).

695 4. Bycroft, C. *et al.* The UK Biobank resource with deep phenotyping and
696 genomic data. *Nature* **562**, 203–209 (2018).

697 5. Chua, S. Y. L. *et al.* Cohort profile: design and methods in the eye and
698 vision consortium of UK Biobank. *BMJ Open* **9**, e025077 (2019).

699 6. Bouma, B. E. *et al.* Optical coherence tomography. *Nature Reviews*
700 *Methods Primers* **2**, (2022).

701 7. Zouache, M. A. *et al.* Comparison of the morphology of the foveal pit
702 between african and caucasian populations. *Transl Vis Sci Technol* **9**, 1–11
703 (2020).

704 8. Tick, S. *et al.* Foveal shape and structure in a normal population. *Invest*
705 *Ophthalmol Vis Sci* **52**, 5105–5110 (2011).

706 9. Wagner-Schuman, M. *et al.* Race- and sex-related differences in retinal
707 thickness and foveal pit morphology. *Invest Ophthalmol Vis Sci* **52**, 625–
708 634 (2011).

709 10. Dubis, A. M., McAllister, J. T. & Carroll, J. Reconstructing foveal pit
710 morphology from optical coherence tomography imaging. *British Journal of*
711 *Ophthalmology* **93**, 1223–1227 (2009).

712 11. De Moraes, C. G. *et al.* Interindividual variations in foveal anatomy and
713 artifacts seen on inner retinal probability maps from spectral domain OCT
714 scans of the macula. *Transl Vis Sci Technol* **7**, (2018).

715 12. O'Sullivan, M. L. *et al.* Foveal differentiation and inner retinal displacement
716 are arrested in extremely premature infants. *Invest Ophthalmol Vis Sci* **62**,
717 (2021).

718 13. Olvera-Barrios, A. *et al.* Foveal Curvature and Its Associations in UK
719 Biobank Participants. *Invest Ophthalmol Vis Sci* **63**, (2022).

720 14. Romero-Bascones, D. *et al.* Spatial characterization of the effect of age
721 and sex on macular layer thicknesses and foveal pit morphology. *PLoS*
722 *One* **17**, (2022).

723 15. Currant, H. *et al.* Sub-cellular level resolution of common genetic variation
724 in the photoreceptor layer identifies continuum between rare disease and
725 common variation. *PLoS Genet* **19**, (2023).

726 16. Currant, H. *et al.* Genetic variation affects morphological retinal phenotypes
727 extracted from UK Biobank optical coherence tomography images. *PLoS*
728 *Genet* **17**, (2021).

729 17. Gao, X. R., Huang, H. & Kim, H. Genome-wide association analyses
730 identify 139 loci associated with macular thickness in the UK Biobank
731 cohort. *Hum Mol Genet* **28**, 1162–1172 (2019).

732 18. Sergouniotis, P. I. *et al.* Autoencoder-based phenotyping of ophthalmic
733 images highlights genetic loci influencing retinal morphology and provides
734 informative biomarkers. *Bioinformatics* **41**, (2024).

735 19. Jackson, V. E. *et al.* Multi-omic spatial effects on high-resolution AI-derived
736 retinal thickness. *Nat Commun* **16**, 1317 (2025).

20. Maryam Zekavat, S. *et al.* Phenome-and genome-wide analyses of retinal optical coherence tomography images identify links between ocular and systemic health. *Sci. Transl. Med* **16**, 4517 (2024).

21. Rajesh, A. E. *et al.* Machine learning derived retinal pigment score from ophthalmic imaging shows ethnicity is not biology. *Nature Communications* **16**, (2025).

22. Mbatchou, J. *et al.* Computationally efficient whole-genome regression for quantitative and binary traits. *Nat Genet* **53**, 1097–1103 (2021).

23. Yang, J. *et al.* Conditional and joint multiple-SNP analysis of GWAS summary statistics identifies additional variants influencing complex traits. *Nat Genet* **44**, 369–375 (2012).

24. Bulik-Sullivan, B. *et al.* LD score regression distinguishes confounding from polygenicity in genome-wide association studies. *Nat Genet* **47**, 291–295 (2015).

25. Appukuttan, B., Giridhar, A., Gopalakrishnan, M. & Sivaprasad, S. Normative spectral domain optical coherence tomography data on macular and retinal nerve fiber layer thickness in Indians. *Indian J Ophthalmol* **62**, 316–321 (2014).

26. Wu, J. *et al.* Clinical science Macular thickness and its associated factors in a Chinese rural adult population: the Handan Eye Study. *Br J Ophthalmol* **107**, 1864–1872 (2023).

27. *Using Population Descriptors in Genetics and Genomics Research*. (National Academies Press, Washington, D.C., 2023). doi:10.17226/26902.

28. Babaker, R. *et al.* Risk factors for age-related macular degeneration: Updated systematic review and meta-analysis. *Medicine (United States)* **104**, e41599 (2025).

763 29. Maugeri, A., Barchitta, M. & Agodi, A. The association between
764 complement factor H rs1061170 polymorphism and age-related macular
765 degeneration: a comprehensive meta-analysis stratified by stage of
766 disease and ethnicity. *Acta Ophthalmol* **97**, e8–e21 (2019).

767 30. Ross, R. J. *et al.* The LOC387715 Polymorphism and Age-Related Macular
768 Degeneration: Replication in Three Case-Control Samples. *Invest*
769 *Ophthalmol Vis Sci* **48**, 1128–1132 (2007).

770 31. Shahid, H. *et al.* Age-related macular degeneration: the importance of
771 family history as a risk factor. *British Journal of Ophthalmology* **96**, 427–
772 431 (2012).

773 32. Curcio, C. A., Kar, D., Owsley, C., Sloan, K. R. & Ach, T. Age-Related
774 Macular Degeneration, a Mathematically Tractable Disease. *Invest*
775 *Ophthalmol Vis Sci* **65**, (2024).

776 33. Lejoyeux, R. *et al.* Genetic analysis of participants with foveal hypoplasia.
777 *Ophthalmic Genet* 1–4 (2025) doi:10.1080/13816810.2025.2520411.

778 34. Bakker, R. *et al.* The retinal pigmentation pathway in human albinism: Not
779 so black and white. *Prog Retin Eye Res* **91**, (2022).

780 35. Ayala, G. D. *et al.* Assessing foveal structure in individuals with TYR
781 R402Q and S192Y hypomorphic alleles. *Ophthalmology Science* **1**,
782 100077 (2021).

783 36. Jones, W. D. *et al.* De novo mutations in MLL cause Wiedemann-Steiner
784 syndrome. *Am J Hum Genet* **91**, 358–364 (2012).

785 37. Choi, J., Joisher, H. N. V., Gill, H. K., Lin, L. & Cepko, C. Characterization
786 of the development of the high-acuity area of the chick retina. *Dev Biol* **511**,
787 39–52 (2024).

788 38. da Silva, S. & Cepko, C. L. Fgf8 expression and degradation of retinoic
789 acid are required for patterning a high-acuity area in the retina. *Dev Cell*
790 **42**, 68-81.e6 (2017).

791 39. Taneera, J. *et al.* Unraveling the significance of PPP1R1A gene in
792 pancreatic β-cell function: A study in INS-1 cells and human pancreatic
793 islets. *Life Sci* **345**, (2024).

794 40. Keane, P. A. *et al.* Optical coherence tomography in the UK Biobank study
795 - Rapid automated analysis of retinal thickness for large population-based
796 studies. *PLoS One* **11**, (2016).

797 41. Xie, Y. *et al.* FGF/FGFR signaling in health and disease. *Signal Transduct*
798 *Target Ther* **5**, (2020).

799 42. Xu, X. *et al.* Fibroblast growth factor receptor 2 (FGFR2)-mediated
800 reciprocal regulation loop between FGF8 and FGF10 is essential for limb
801 induction. *Development* **125**, 753–765 (1998).

802 43. Tomita, H. *et al.* The Protein Tyrosine Phosphatase Receptor Delta
803 Regulates Developmental Neurogenesis. *Cell Rep* **30**, 215-228.e5 (2020).

804 44. Badde, A., Bumsted-O'Brien, K. M. & Schulte, D. Chick receptor protein
805 tyrosine phosphatase λ/ψ (cRPTPλ/cRPTPψ) is dynamically expressed at
806 the midbrain-hindbrain boundary and in the embryonic neural retina. *Gene*
807 *Expression Patterns* **5**, 786–791 (2005).

808 45. Woertz, E. N. *et al.* Quantitative Foveal Structural Metrics as Predictors of
809 Visual Acuity in Human Albinism. *Invest Ophthalmol Vis Sci* **65**, (2024).

810 46. Wilk, M. A. *et al.* Relationship between foveal cone specialization and pit
811 morphology in Albinism. *Invest Ophthalmol Vis Sci* **55**, 4186–4198 (2014).

812 47. Kreis, J. & Carroll, J. Applications of Adaptive Optics Imaging for Studying
813 Conditions Affecting the Fovea. *Annu Rev Vis Sci* **35**, 239–262 (2024).

814 48. Sampson, D. M., Dubis, A. M., Chen, F. K., Zawadzki, R. J. & Sampson, D.
815 D. Towards standardizing retinal optical coherence tomography
816 angiography: a review. *Light Sci Appl* **11**, 63 (2022).

817 49. Dubis, A. M. *et al.* Relationship between the foveal avascular zone and
818 foveal pit morphology. *Invest Ophthalmol Vis Sci* **53**, 1628–1636 (2012).

819 50. Yan, Q. *et al.* Deep-learning-based prediction of late age-related macular
820 degeneration progression. *Nat Mach Intell* **2**, 141–150 (2020).

821 51. Warwick, A. N. *et al.* UK Biobank retinal imaging grading: methodology,
822 baseline characteristics and findings for common ocular diseases. *Eye*
823 *(Basingstoke)* **37**, 2109–2116 (2023).

824 52. Munafò, M. R., Tilling, K., Taylor, A. E., Evans, D. M. & Smith, G. D.
825 Collider scope: When selection bias can substantially influence observed
826 associations. *Int J Epidemiol* **47**, 226–235 (2018).

827 53. Schoeler, T. *et al.* Participation bias in the UK Biobank distorts genetic
828 associations and downstream analyses. *Nat Hum Behav* **7**, 1216–1227
829 (2023).

830 54. Patel, P. J. *et al.* Spectral-domain optical coherence tomography imaging
831 in 67 321 adults: Associations with macular thickness in the UK biobank
832 study. *Ophthalmology* **123**, 829–840 (2016).

833 55. Julian, T., Fitzgerald, T., Birney, E. & Sergouniotis, P. I. Pigmentation and
834 retinal pigment epithelium thickness: a study of the phenotypic and
835 genotypic relationships between ocular and extraocular pigmented tissues.
836 Preprint at https://doi.org/10.1101/2024.12.04.626809 (2024).

837 56. Zhou, Y. *et al.* AutoMorph: automated retinal vascular morphology
838 quantification via a deep learning pipeline. *Transl Vis Sci Technol* **11**,
839 (2022).

840 57. Romero-Bascones, D. *et al.* Foveal pit morphology characterization: A
841 quantitative analysis of the key methodological steps. *Entropy* **23**, (2021).

842 58. Constantinescu, A. E. *et al.* A framework for research into continental
843 ancestry groups of the UK Biobank. *Hum Genomics* **16**, (2022).

844 59. Auton, A. *et al.* A global reference for human genetic variation. *Nature* vol.
845 526 68–74 Preprint at https://doi.org/10.1038/nature15393 (2015).

846 60. Purcell, S. *et al.* PLINK: A tool set for whole-genome association and
847 population-based linkage analyses. *Am J Hum Genet* **81**, 559–575 (2007).

848 61. Alexander, D. H., Novembre, J. & Lange, K. Fast model-based estimation
849 of ancestry in unrelated individuals. *Genome Res* **19**, 1655–1664 (2009).

850 62. Cunningham, F. *et al.* Ensembl 2022. *Nucleic Acids Res* **50**, D988–D995
851 (2022).

852 63. Ochoa, D. *et al.* Open Targets Platform: Supporting systematic drug-target
853 identification and prioritisation. *Nucleic Acids Res* **49**, D1302–D1310
854 (2021).

855 64. Sollis, E. *et al.* The NHGRI-EBI GWAS Catalog: knowledgebase and
856 deposition resource. *Nucleic Acids Res* **51**, D977–D985 (2023).

857 65. Myers, T. A., Chanock, S. J. & Machiela, M. J. LDlinkR: An R Package for
858 Rapidly Calculating Linkage Disequilibrium Statistics in Diverse
859 Populations. *Front Genet* **11**, (2020).

860 66. Bulik-Sullivan, B. *et al.* LD score regression distinguishes confounding from
861 polygenicity in genome-wide association studies. *Nat Genet* **47**, 291–295
862 (2015).

863 67. Davidson-Pilon, C. lifelines: survival analysis in Python. *J Open Source*
864 *Softw* **4**, 1317 (2019).

68. Seabold, S. & Perktold, J. Statsmodels: Econometric and Statistical Modeling with Python. *Proceeding of the 9th Python in Science Conference* (2010).

69. Burgess, S., Butterworth, A. & Thompson, S. G. Mendelian randomization analysis with multiple genetic variants using summarized data. *Genet Epidemiol* **37**, 658–665 (2013).

70. Hemani, G. *et al.* The MR-Base platform supports systematic causal inference across the human phenome. *Elife* **7**, (2018).

71. Bowden, J. *et al.* Improving the visualization, interpretation and analysis of two-sample summary data Mendelian randomization via the Radial plot and Radial regression. *Int J Epidemiol* **47**, 1264–1278 (2018).

72. Burgess, S. & Thompson, S. G. Interpreting findings from Mendelian randomization using the MR-Egger method. *Eur J Epidemiol* **32**, 377–389 (2017).

73. Burgess, S. *et al.* Guidelines for performing Mendelian randomization investigations. *Wellcome Open Res* **4**, 186 (2019).

ACKNOWLEDGEMENTS

We acknowledge the following sources of funding: the Wellcome Trust (224643/Z/21/Z, Clinical Research Career Development Fellowship to P.I.S.); the UK National Institute for Health Research (NIHR) Clinical Lecturer Programme (CL-2017-06-001 to P.I.S.); the NIHR Manchester Biomedical Research Centre (NIHR 203308 to P.I.S. and G.C.B.); the EMBL European Bioinformatics Institute (EMBL-EBI) (S.T., T.F. and E.B.); and the Howard Hughes Medical Institute (C.L.C). Research reported in this publication was supported in part by the National Eye Institute of the National Institutes of Health (NIH) under award numbers R01EY017607 and R01EY033580. The content is solely the responsibility of the authors and does not necessarily represent the official views of the NIH.

The UK Biobank Eye and Vision Consortium is supported by funding from the NIHR Biomedical Research Centre at Moorfields Eye Hospital and UCL Institute of Ophthalmology, the Alcon Foundation and the Desmond Foundation. The complete list of members of this Consortium can be found in the Supplementary Information.

AUTHOR CONTRIBUTIONS STATEMENT

P.I.S. conceived and designed the experiments. The UK Biobank Eye and Vision Consortium, D.R., H.N.V.J., U.A., M.B., T.F., E.B., C.L.C., J.C. and P.I.S provided datasets and analytical tools. D.J.G., D.R., T.H.J., S.T., H.N.V.J., T.F.,

C.L.C., and P.I.S. analyzed the data. D.J.G. wrote the manuscript with support from P.I.S. All authors critically revised and approved the manuscript.

COMPETING INTERESTS STATEMENT

E.B. is a paid consultant and equity holder of Oxford Nanopore, a paid consultant to Dovetail, and a non-executive director of Genomics England, a limited company wholly owned by the UK Department of Health and Social Care. All other authors declare no competing interests. D.R. is an employee of RetinAI, but performed this work independently of RetinAI.

914 **UK Biobank Eye and Vision Consortium**

915

916 Jay E. Self,[9,10] Graeme C. Black[1,11], Panagiotis I. Sergouniotis[1,3,5,11]

917

918 [1] Division of Evolution, Infection and Genomics, School of Biological Sciences,

919 Faculty of Biology, Medicine and Health, University of Manchester, Manchester,

920 UK.

921

922 [3] Manchester Royal Eye Hospital, Manchester University NHS Foundation Trust,

923 Manchester, UK.

924

925 [9] Clinical and Experimental Sciences, Faculty of Medicine, University of

926 Southampton, Southampton, UK

927

928 [10] Southampton Eye Unit, University Hospital Southampton NHS Foundation

929 Trust, Southampton, UK

930

931 [11] Manchester Centre for Genomic Medicine, Saint Mary's Hospital, Manchester

932 University NHS Foundation Trust, Manchester, UK

933

934 A full list of members appears in the Supplementary Information.

935

1

En Face | **Section** | **OCT**

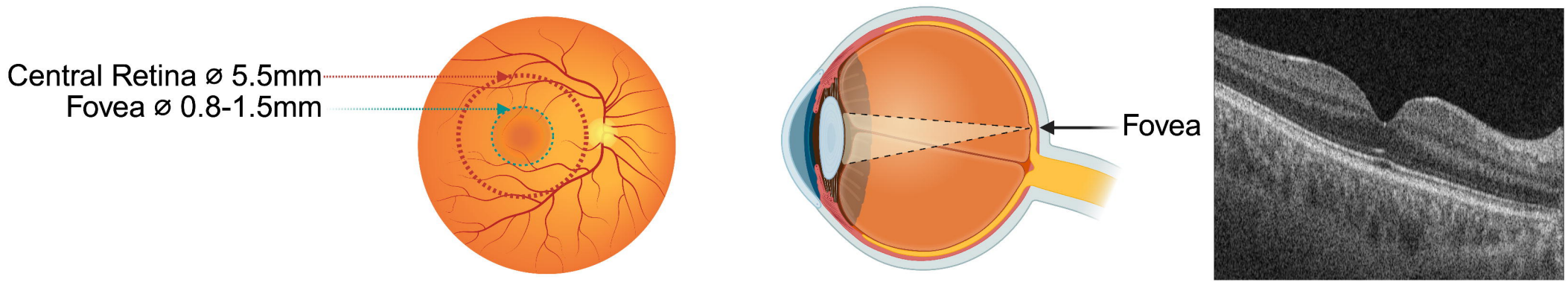

2

biobank uk

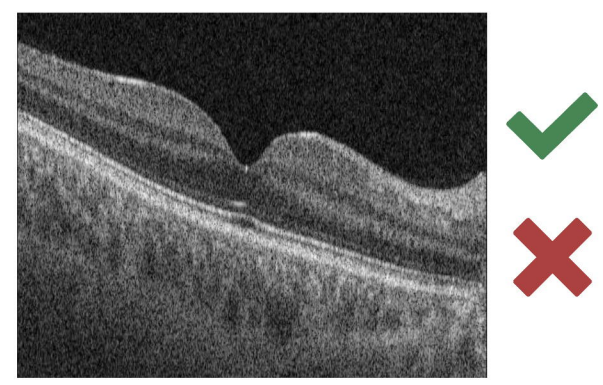

Quality control

3

RETIMAT
Retinal image analysis in MATLAB

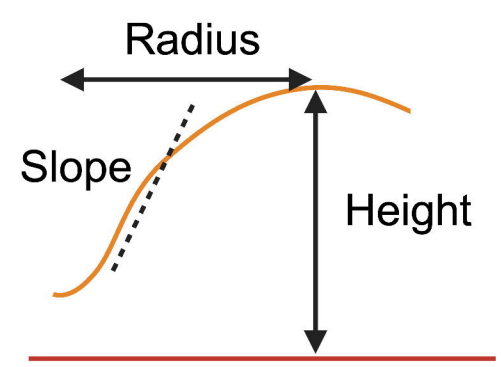

Foveal morphological parameter extraction:
pit volume, rim radius, rim height, mean slope, pit depth, CFT

4

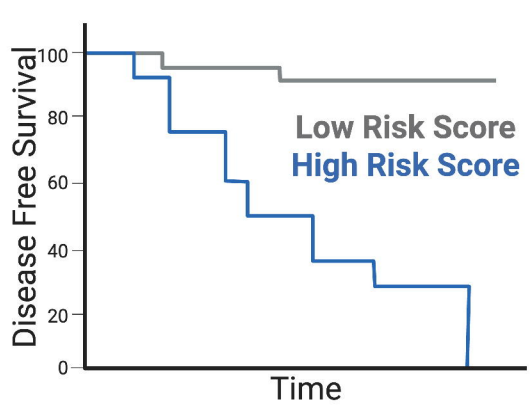

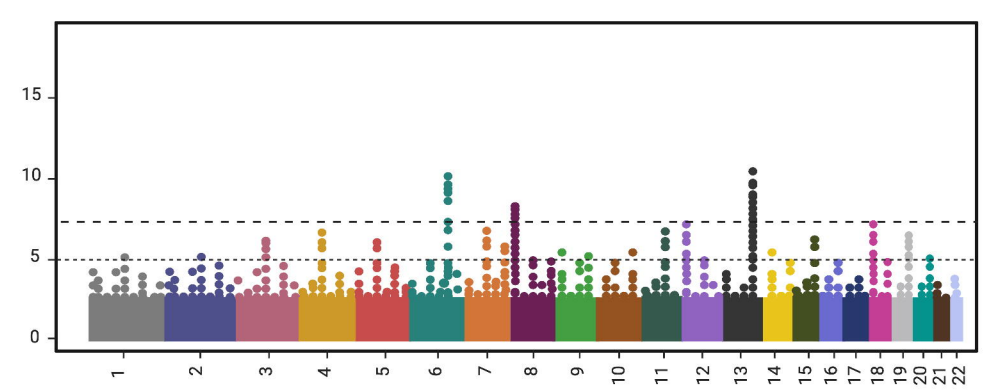

Foveal phenotype studies:

- Phenotypic associations
- Time-to-event analysis

Genetic studies:

- Genetic associations
- Heritability estimates
- Genetic correlation

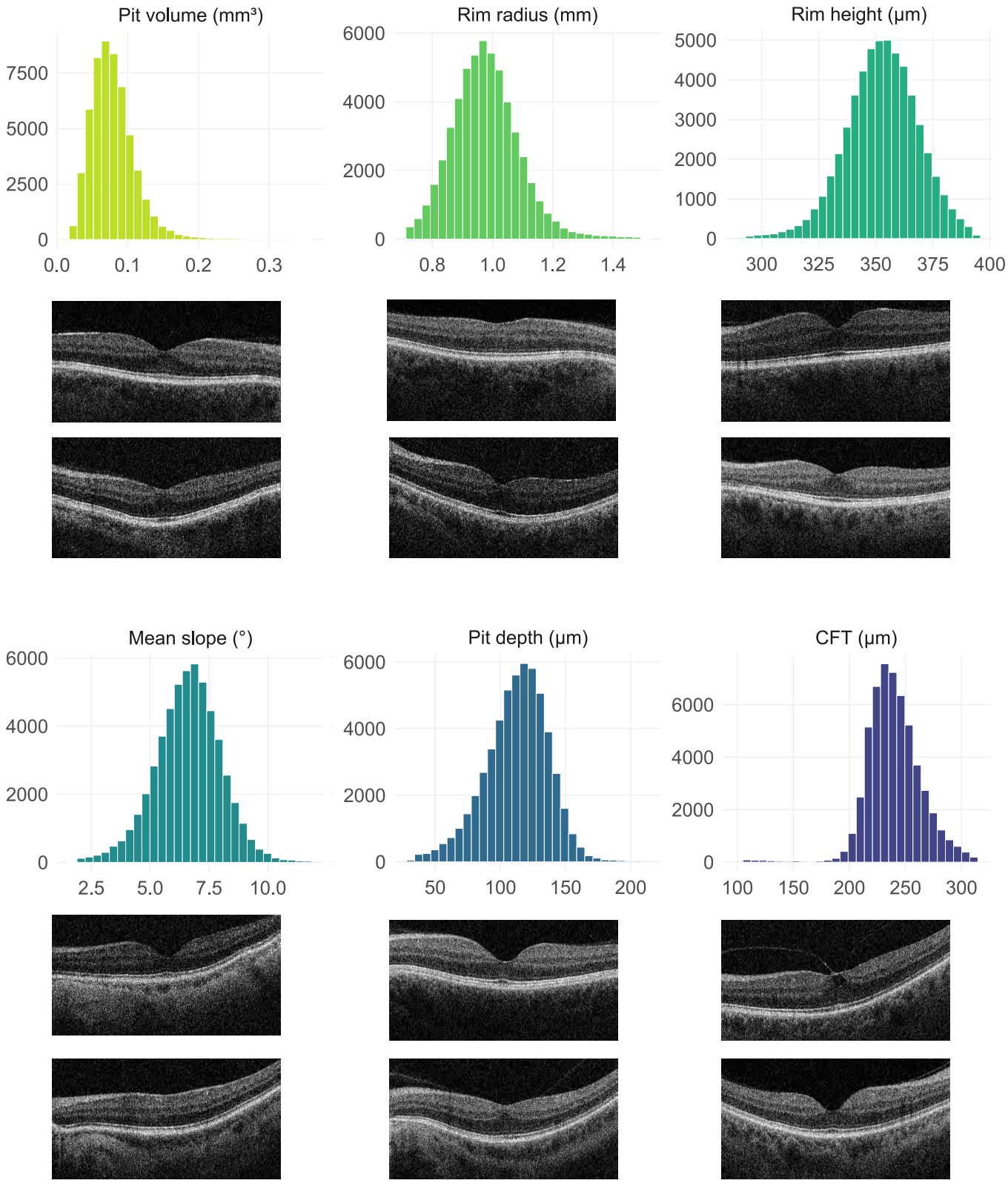
Pit volume (mm³)
7500
5000
2500
0
0.0
0.1
0.2
0.3
Rim radius (mm)
6000
4000
2000
0
0.8
1.0
1.2
1.4
Rim height (µm)
5000
4000
3000
2000
1000
0
300
325
350
375
400
Mean slope (°)
6000
4000
2000
0
2.5
5.0
7.5
10.0
Pit depth (µm)
6000
4000
2000
0
50
100
150
200
CFT (µm)
6000
4000
2000
0
100
150
200
250
300

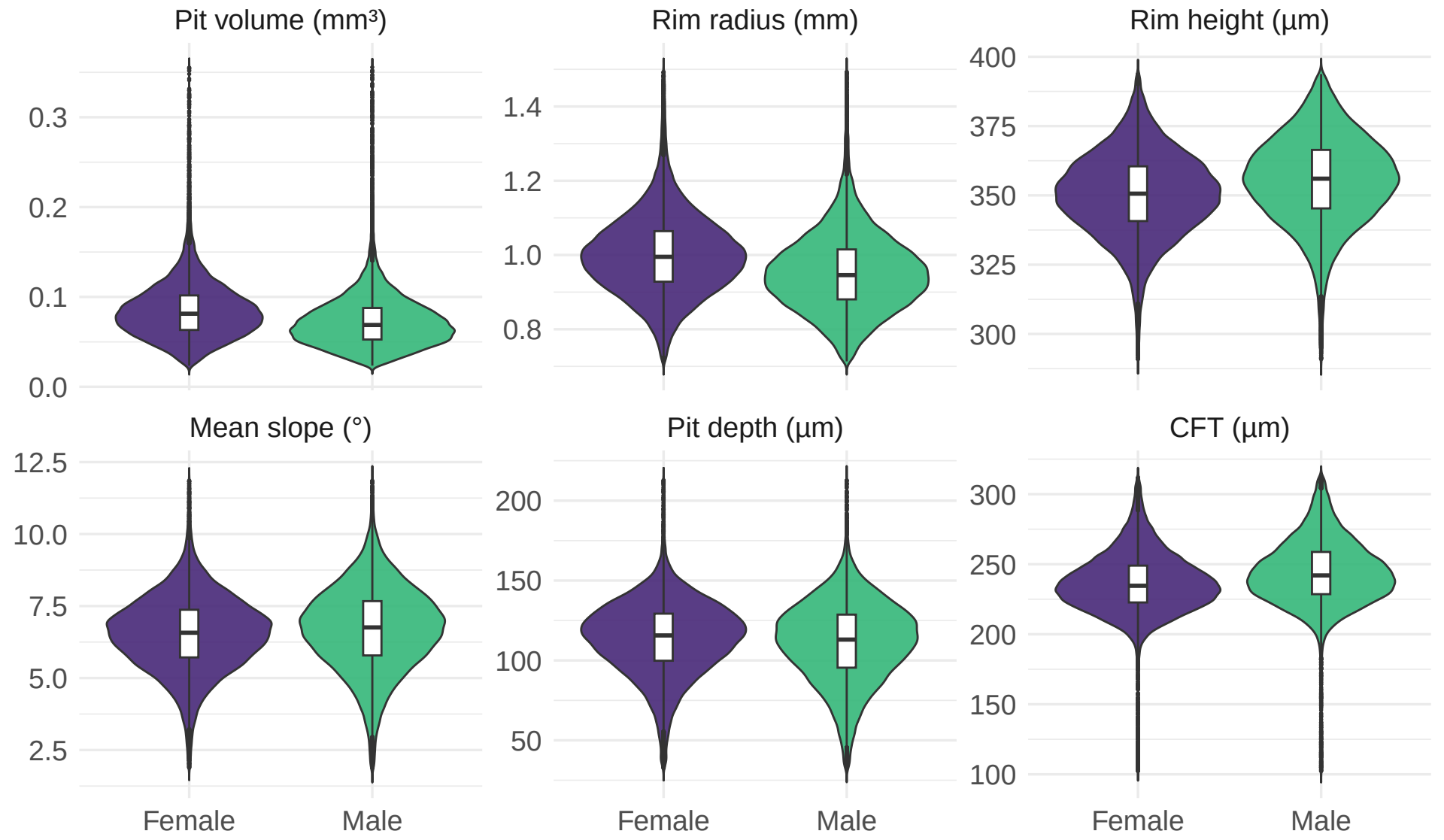
Pit volume (mm³)
0.3
0.2
0.1
0.0
Rim radius (mm)
1.4
1.2
1.0
0.8
Rim height (µm)
400
375
350
325
300
Mean slope (°)
12.5
10.0
7.5
5.0
2.5
Pit depth (µm)
200
150
100
50
CFT (µm)
300
250
200
150
100
Female
Male
Female
Male
Female
Male

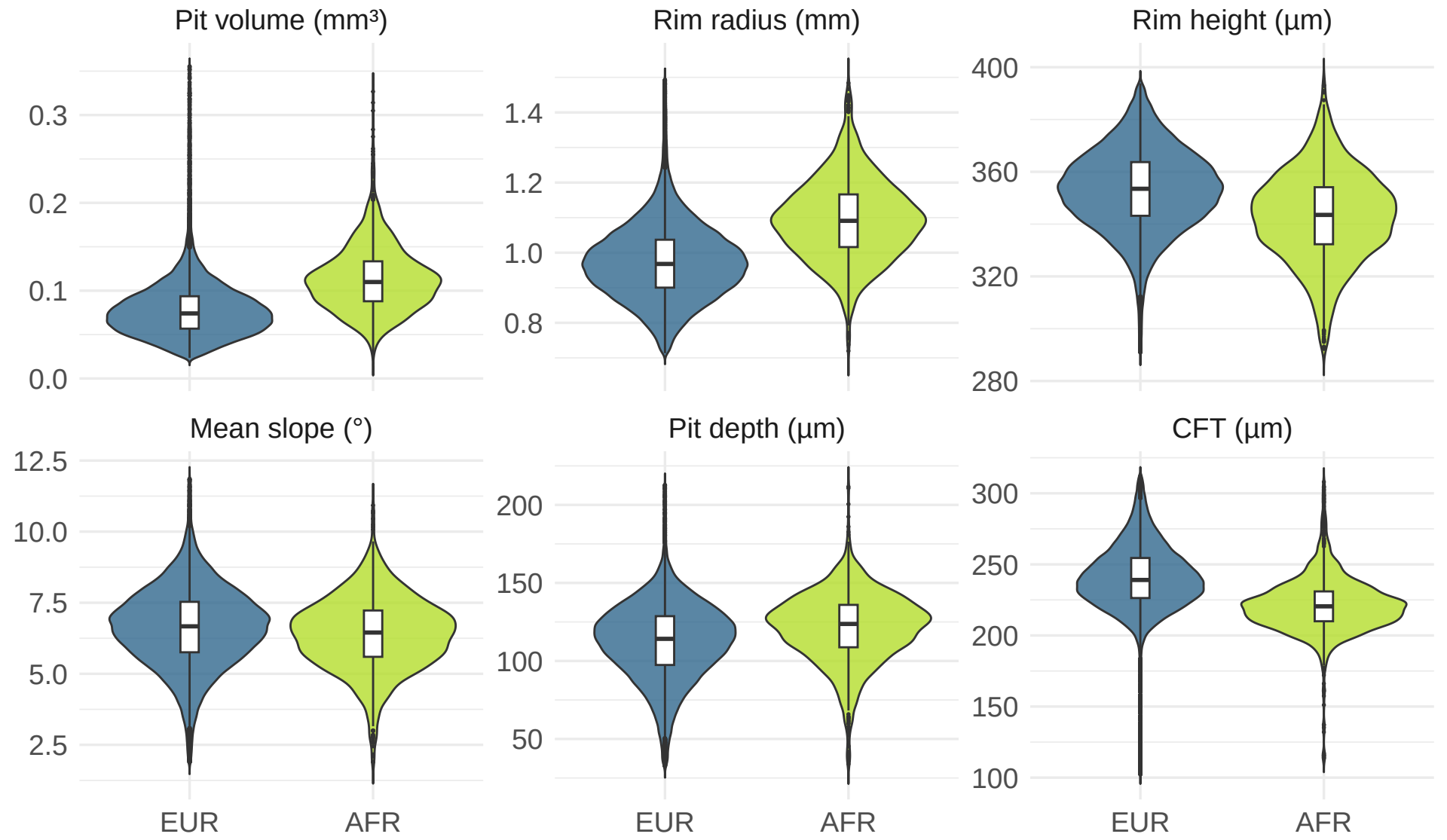
Pit volume (mm³)
0.3
0.2
0.1
0.0
Rim radius (mm)
1.4
1.2
1.0
0.8
Rim height (µm)
400
360
320
280
Mean slope (°)
12.5
10.0
7.5
5.0
2.5
Pit depth (µm)
200
150
100
50
CFT (µm)
300
250
200
150
100
EUR
AFR
EUR
AFR
EUR
AFR

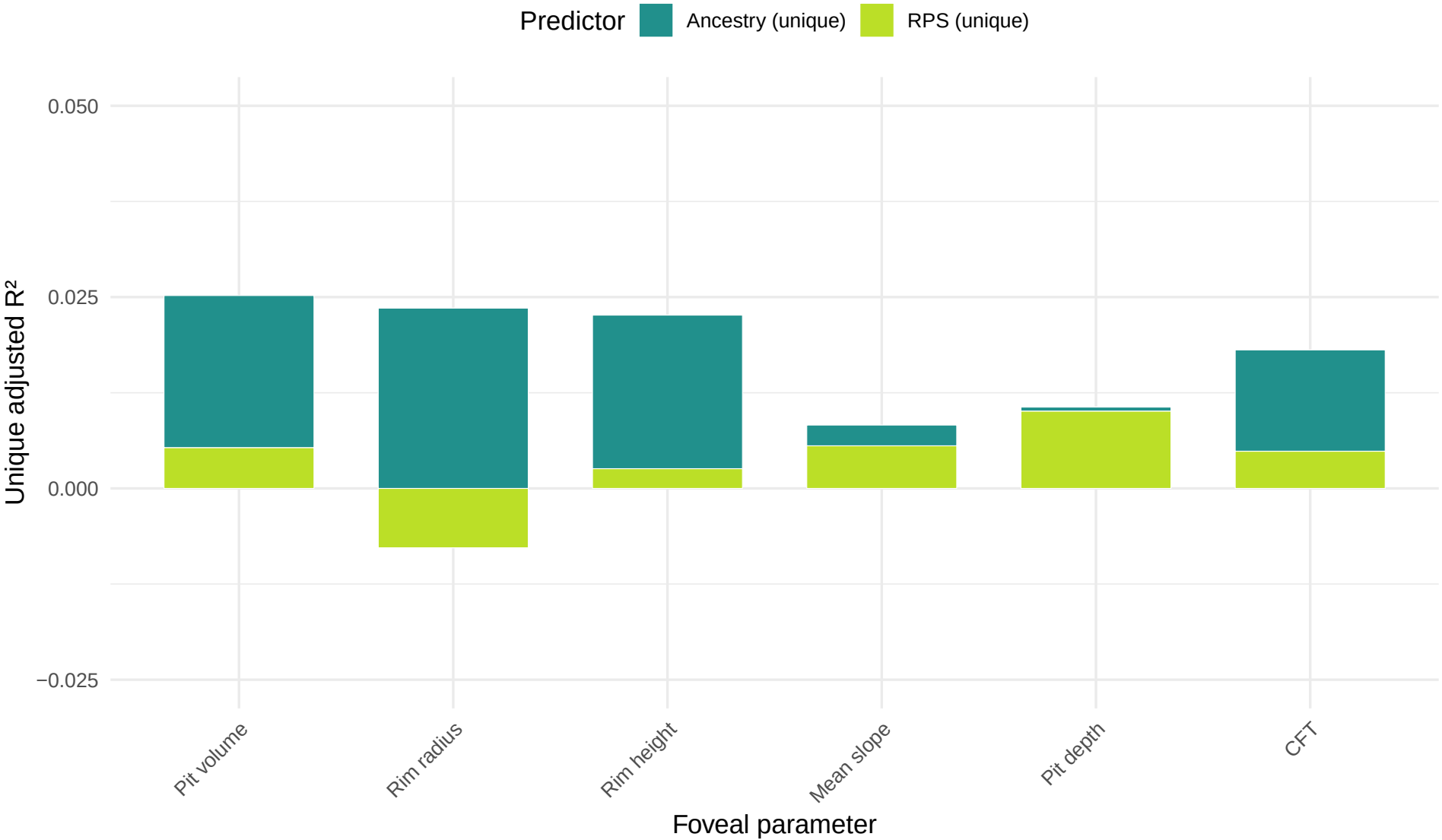
Predictor
Ancestry (unique)
RPS (unique)
0.050
0.025
0.000
−0.025
Unique adjusted R²
Pit volume
Rim radius
Rim height
Mean slope
Pit depth
CFT
Foveal parameter

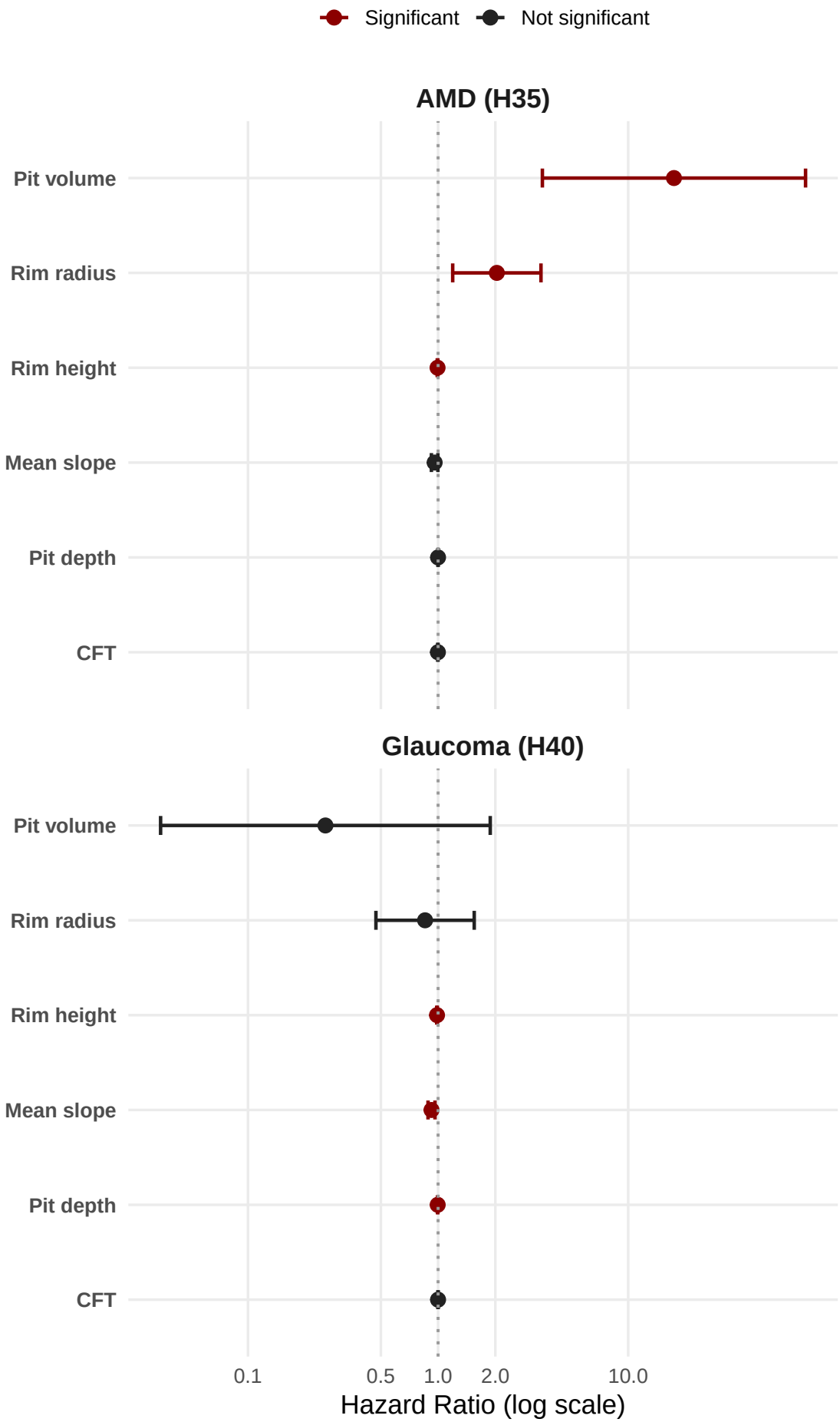
Significant
Not significant
AMD (H35)
Pit volume
Rim radius
Rim height
Mean slope
Pit depth
CFT
Glaucoma (H40)
Pit volume
Rim radius
Rim height
Mean slope
Pit depth
CFT
0.1
0.5
1.0
2.0
10.0
Hazard Ratio (log scale)

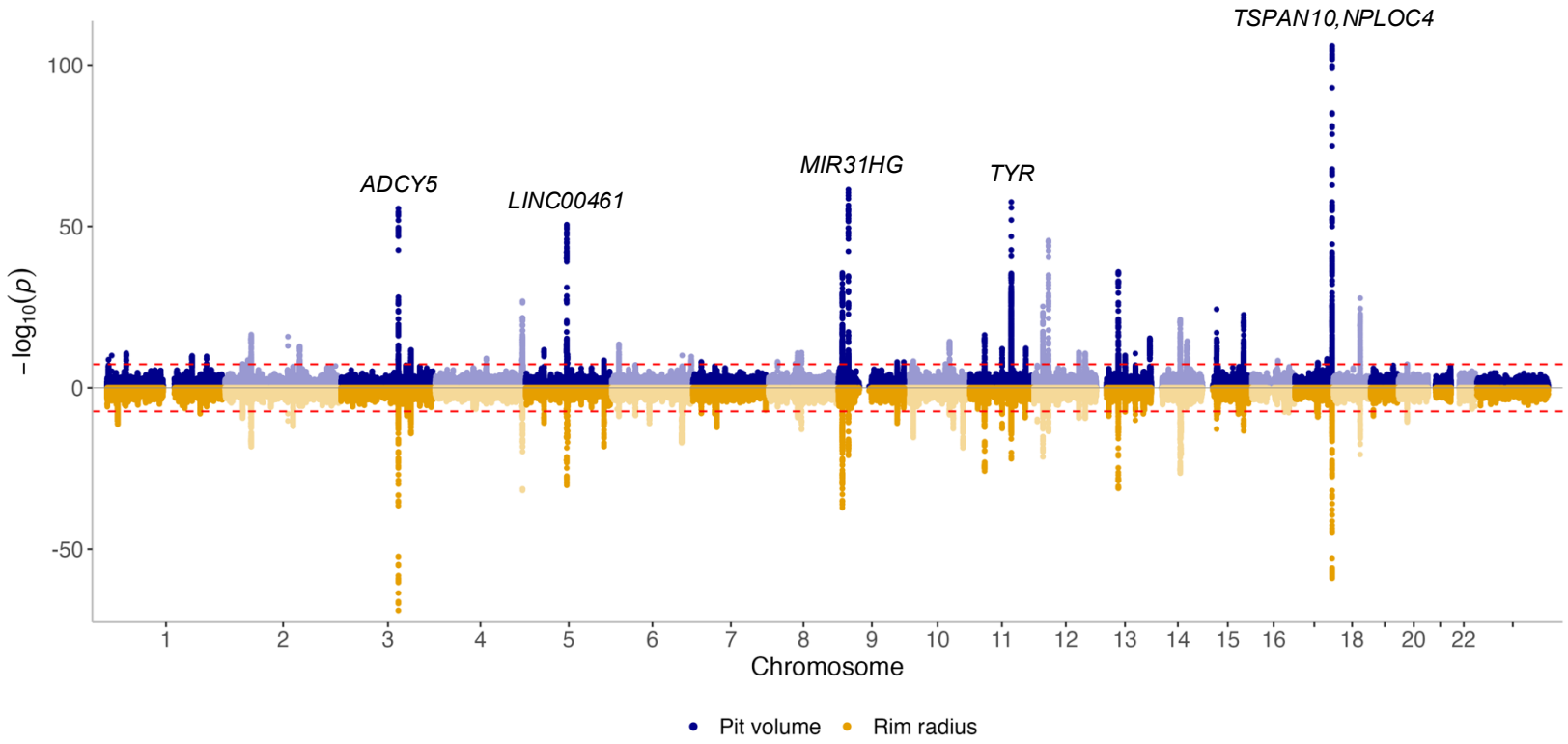
TSPAN10,NPLOC4
ADCY5
LINC00461
MIR31HG
TYR
100
50
0
-50
$-\log_{10}(p)$
1
2
3
4
5
6
7
8
9
10
11
12
13
14
15
16
18
20
22
Chromosome
Pit volume
Rim radius

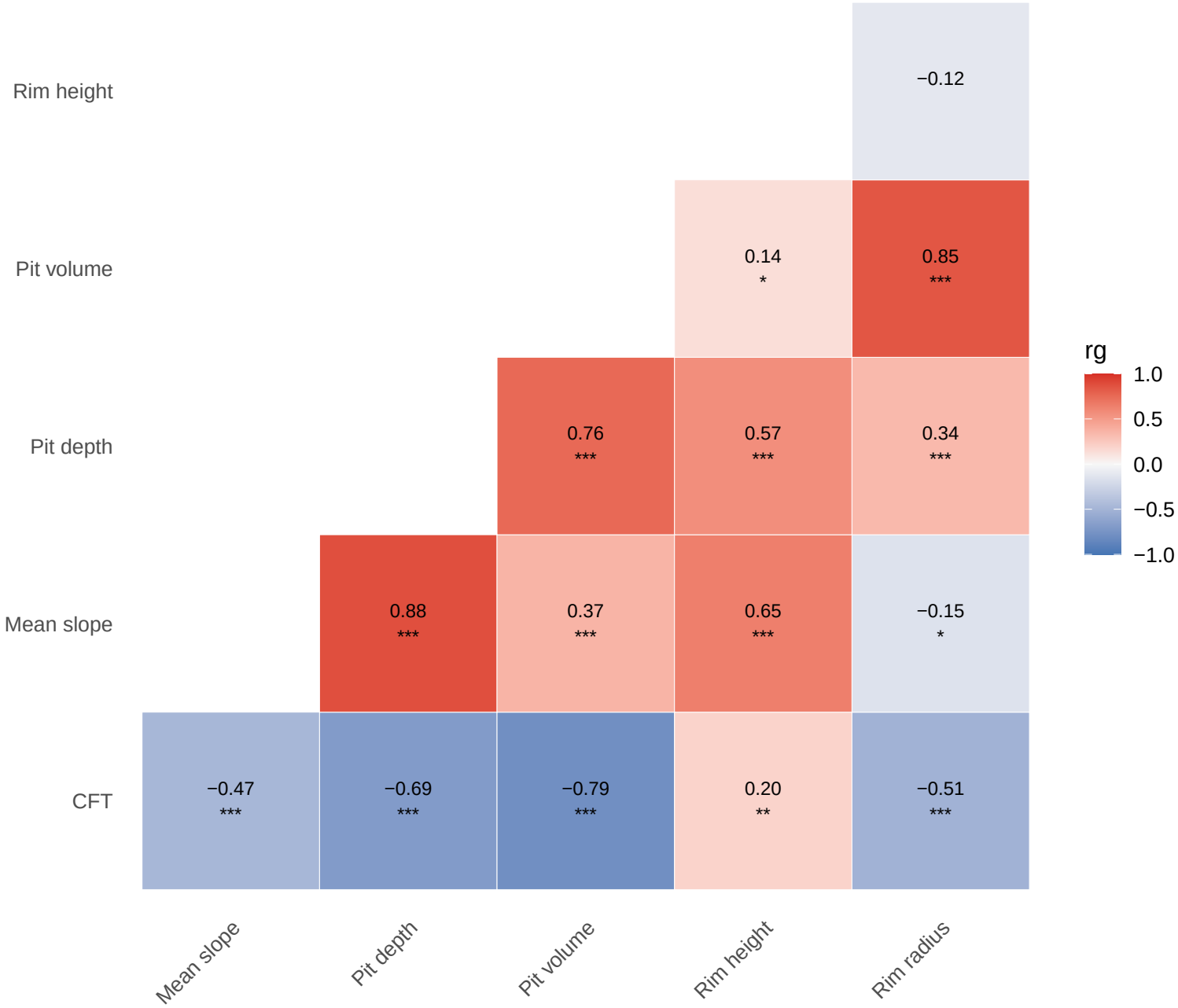
Rim height
Pit volume
Pit depth
Mean slope
CFT
−0.12
0.14
*
0.85
***
0.76
***
0.57
***
0.34
***
0.88
***
0.37
***
0.65
***
−0.15
*
−0.47
***
−0.69
***
−0.79
***
0.20
**
−0.51
***
Mean slope
Pit depth
Pit volume
Rim height
Rim radius
rg
1.0
0.5
0.0
−0.5
−1.0